**NOAA NESDIS
CENTER for SATELLITE APPLICATIONS and
RESEARCH**

Algorithm Theoretical Basis Document For Enterprise Nighttime Cloud Optical Depth, Cloud Particle Size, Cloud Ice Water Path, and Cloud Liquid Water Path

Patrick Minnis, NASA Langley Research Center
Patrick W. Heck, UW-Madison/CIMSS

Version 0.1.0
October 1, 2020

TABLE OF CONTENTS

LIST OF FIGURES

LIST OF TABLES

LIST OF ACRONYMS

ABI - Advanced Baseline Imager
AERI – Atmospheric Emitted Radiance Interferometer
AIT - Algorithm Integration Team
AMF – ARM Mobile Facility
AMSR-2 – Advanced Microwave Scanning Radiometer-2
ARM – Atmospheric Radiation Measurement
ATBD - algorithm theoretical basis document
AVHRR - Advanced Very High Resolution Radiometer
AWG - Algorithm Working Group
BTD - Brightness Temperature Difference
CALIPSO - Cloud-Aerosol Lidar and Infrared Pathfinder Satellite Observations
CARL - Climate Research Facility Raman Lidar
CERES - Clouds and the Earth's Radiant Energy System
CIMSS - Cooperative Institute for Meteorological Satellite Studies
COD - Cloud Optical Depth
CONUS - Continental United States
CPS - Cloud Particle Size
CTT - Cloud Top Temperature
ECMWF - European Centre for Medium-Range Weather Forecasting
F&PS - Function and Performance Specification
GCOM-W – Global Change Observation Mission 1st-Water
GEOPROF - Geometrical Profiling algorithm
GFS - Global Forecast System
GOES - Geostationary Operational Environmental Satellite
IR - InfraRed
IRR - Imaginary Indices of Refraction
IWP - Ice Water Path
LWP - Liquid Water Path
MODIS - Moderate Resolution Imaging Spectroradiometer
NASA - National Aeronautics and Space Administration
NCOMP - Nighttime Cloud Optical and Microphysical Properties
NWP - Numerical Weather Prediction
PFAAST - Pressure layer Fast Algorithm for Atmospheric Transmittances
RO - Radar Only
RTM - Radiative Transfer Model
SEVIRI - Spinning Enhanced Visible and Infrared Imager
SGP - Southern Great Planes
SIR – Solar InfraRed
SIRTA - Site Instrumental de Recherche par Teledetection Atmospheric
SIST - Shortwave-infrared Infrared Split-window Technique
SSEC - Space science and Engineering Center
SNPP – Suomi National Polar-orbiting Partnership
S-W – Split Window

TOA - Top of Atmosphere
UTC – Universal Time Coordinates
UW - University of Wisconsin
VIIRS – Visible Infrared Imaging Radiometer Suite

ABTRACT

The Nighttime Cloud Optical and Microphysical Property Algorithm Theoretical Basis Document details the physical basis for the algorithm to be used to retrieve nighttime water and ice cloud optical depth, particle size and liquid or ice water path from imagery taken by the Visible Infrared Imaging Radiometer Suite aboard JPSS. The algorithm is based primarily on the Solar Infrared Solar-infrared Technique from NASA Langley Research Center, but has been adapted to utilize upstream JPSS products and to function in the JPSS framework. This approach is identical to that used for processing ABI imagery taken aboard GOES-R. Sufficient information is provided to enable the implementation of the algorithm and software development. Validation studies for each of the derived parameters is included thereby exhibiting the algorithm's ability to meet JPSS VIIRS performance specification.

1 INTRODUCTION

1.1 Purpose of This Document

This Algorithm Theoretical Basis Document (ATBD) provides a high-level description of the physical basis for the inference of nighttime water/ice cloud optical depth (COD) and Particle Size (CPS) from imagery taken by the Visible Infrared Imaging Radiometer Suite (VIIRS) and the GOES-R Advance Baseline Imager (ABI). The COD and CPS will be inferred for all nighttime pixels identified as containing cloud by the JPSS VIIRS cloud type, and for which cloud temperature has been obtained. The COD and CPS are used subsequently to calculate liquid water path (LWP) and ice water path (IWP). These parameters can be inter-compared with those derived from active measurements from space-born instruments such as AMSR2 and CALIPSO, as well as from ground-based sensors such as microwave radiometers and from similar parameters derived from using similar algorithms applied to VIIRS data.

1.2 Who Should Use This Document

The intended users of this document are those interested in understanding the physical basis of the algorithms and how to use the output of this algorithm to study or assimilate cloud properties. This document also provides information useful to anyone maintaining or modifying the original algorithm.

1.3 Inside Each Section

This document is broken down into the following main sections.

- **Observing System Overview**: Provides relevant details of the VIIRS.

- **Algorithm Description**: Provides all the detailed description of the algorithm including its physical basis, the mathematical elements, its input and its output.

- **Test Data Sets and Outputs**: Provides examples of algorithm input and output and describes validation efforts.

- **Practical Considerations**: Provides an overview of the processing considerations for the algorithm.

- **Assumptions and Limitations**: Provides an overview of the current limitations of the approach and provides the plan for overcoming these limitations with further algorithm development.

1.4 Related Documents

This document currently does not relate to any other document outside of the specifications of the current JPSS Function and Performance Specification (F&PS) and to the references given throughout.

1.5 Revision History

Version 0.1.0 of this document was created by Patrick Minnis of NASA Langley Research Center, Patrick Heck of CIMSS at University of Wisconsin-Madison and colleagues.

2 OBSERVING SYSTEM OVERVIEW

This section describes the products generated by the VIIRS algorithm for deriving COD, CPS, LWP and/or IWP at night and the requirements it places on the sensor.

2.1 Products Generated

This algorithm is responsible for the calculation of water/ice COD, CPS and water/ice path for all VIIRS nighttime cloudy pixels. In our context, the determination of nighttime is defined to be where the solar zenith angle for a given pixel is greater than or equal to 90°. In addition, these same cloud properties are calculated for solar zenith angles greater than or equal to 82° and less than 90°, but only in a qualitative sense. Another point to keep in mind is that the current algorithm design utilizes cloud phase (inferred from VIIRS cloud type) and cloud top temperature. Cloud types and cloud top temperatures are determined by VIIRS algorithms that must be invoked prior to running the algorithm. An attempt will be made to derive COD, CPS, LWP and/or IWP for all pixels that are cloudy with quality flags indicating the degree of success. Units and additional details for the derived quantities are given in 3.4.3.1.

The performance of the algorithm will be sensitive to such issues as sensor or imagery artifacts, instrument noise and imperfections in the knowledge of the sensor response functions. Calibrated observations are critical because the technique utilizes the observed values in conjunction with calculations from a radiative transfer model where accurate radiances are assumed. The channel specifications are given in the current F&PS with pertinent descriptors extracted below in Table 1. These measurement ranges, accuracies and precisions apply to the CONUS, full disk and mesoscale Product Geographical Ranges.

In Table 1 the current F&PS requirements are in black while the F&PS requirements that are awaiting approval by the GSP are given in red. This ATBD assumes that the pending requirements will be approved, so our validation studies were performed with that in mind.

Table 1. Key F&PS product requirements for NCOMP.

Observational Requirement	LEVEL[1]	Geographic Coverage[2]	Horiz. Res.	Mapping Accuracy	Msmnt. Range (liquid / ice)	Msmnt. Accuracy (liquid / ice)	Msmnt. Precision (K)	Refresh Rate	Extent Qualifier[3]
Cloud Optical Depth	T	C	2 km	1 km	1-5	30%	max of 0.8 or 30%	15 min	VZA <65
Cloud Particle Size	CT	C	2 km	1 km	2-32 μm 2-50 μm	Greater of 4μm or 30% 10μm	Greater of 4μm or 25% Greater of 10μm of 25%	5 min	VZA <65
Liquid Water Path	T	C	2 km	1 km	25-100 g/m2	Greater of 25 g/m^2 or 15%	Greater of 25 g/m^2 or 40%	5 min	VZA <65
Ice Water Path	T	C	2 km	1 km	25-175 g/m2	Greater of 25 g/m^2 or 30%	Greater of 25 g/m^2 or 40%	5 min	VZA <65

1-T – total column, CT- cloud top, 2-C-Conus, FD- Full disk, M – Mesoscale, 3- VZA- viewing zenith angle qualifier

2.2   Instrument Characteristics

Table 2 summarizes the VIIRS channels used in the algorithm that determines the nighttime cloud optical and microphysical properties. The final channel set may vary as the algorithm continues to mature, but for the 100% version of the code and this ATBD the channels are as indicated. This version of the algorithm uses channels 3.9μm, 11μm and 12μm.

Table 2. Channel numbers and wavelengths for VIIRS channels used in current or future algorithm. ✓ indicates usage in current algorithm while # indicates possible future use.

Wavelength (μm)	Used in Algorithm
3.7	✓
8.55	#
10.76	✓
12.01	✓

3 ALGORITHM DESCRIPTION

Below is complete description of the algorithm at its current level of maturity.

3.1 Algorithm Overview

The COD (τ) and CPS (r_e) are critical for determining the liquid and ice water content of clouds, which impact numerical weather and climate models, as well as any calculations of heating rates and radiative fluxes. The VIIRS and ABI approachs for inferring nighttime COD, CPS, LWP and IWP is based on a heritage algorithm from NASA Langley Research Center (Minnis et al. 1995, 2009) that is being used to derive nighttime cloud properties from MODIS imagery for the CERES project, GOES, AVHRR and MTSAT imagery, as well as from other narrowband radiometers aboard other satellites and for a variety of other projects.

The current algorithm, from this point forward referred to as the Nighttime Cloud Optical and Microphysical Properties (NCOMP) algorithm, will use 3.9µm, 11µm and 12µm.

3.2 Processing Outline

The processing outline of the NCOMP retrieval algorithm is summarized in Figure 1. The current NCOMP algorithm has been implemented in both online and offline frameworks, at CIMSS and by the AIT, respectively. For development purposes, the offline framework's routines are used to provide all of the observations and ancillary data, although the usage of other frameworks is possible assuming all inputs and ancillary data are supplied. The NCOMP algorithm can run on segments of data, as all algorithms in the offline framework do, but can also run on individual pixels if all of the input data and ancillary data sets are available. A segment is comprised of multiple scan lines.
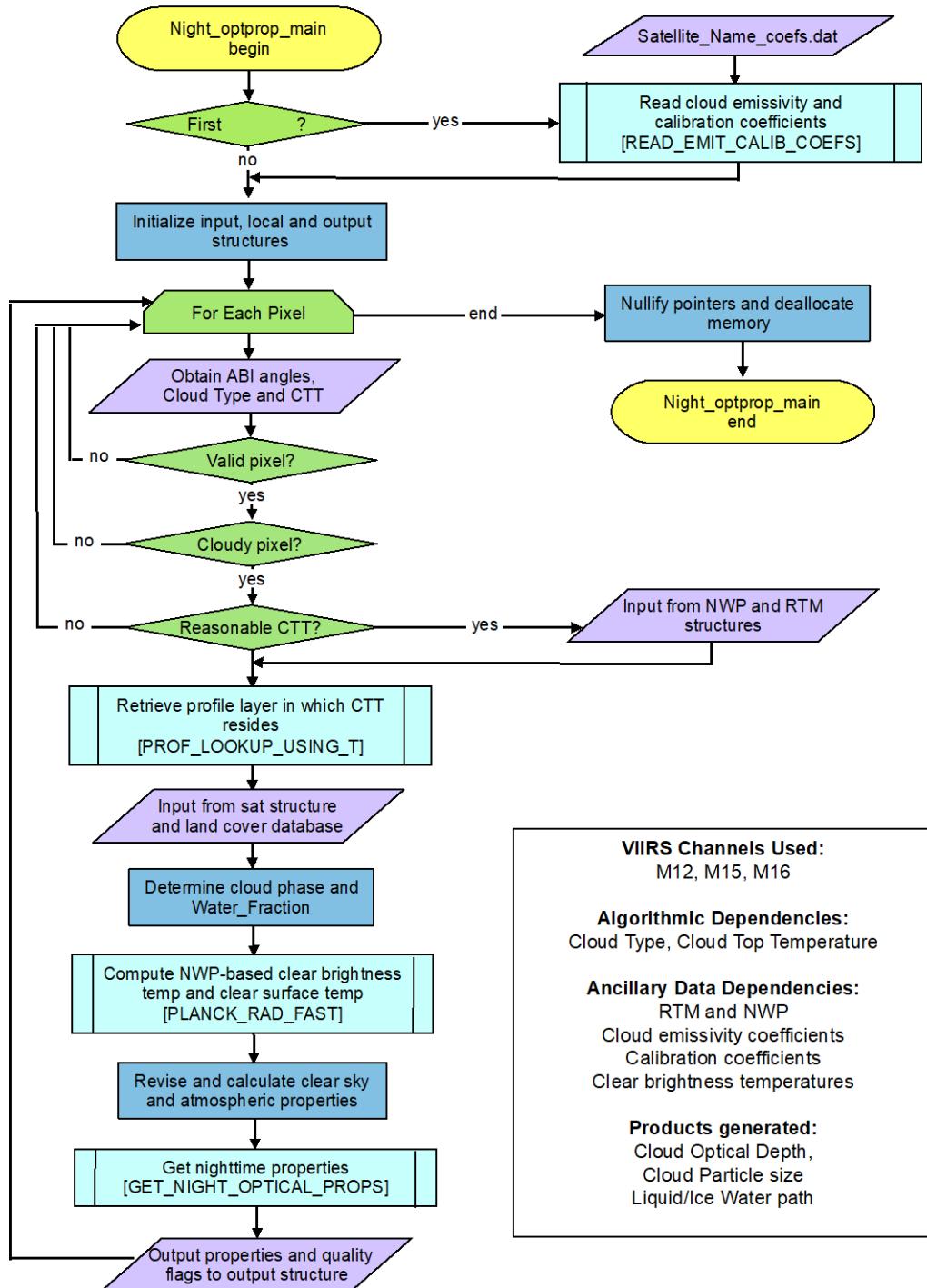
Figure 1. High level flowchart of the Nighttime Cloud Optical and Microphysical Properties algorithm illustrating the main processing sections

3.3   Algorithm Input

This section describes the input needed to invoke and process VIIRS data with the NCOMP algorithm.

3.3.1   Primary Sensor Data

The list below contains the primary sensor data used by the NCOMP algorithm. By primary sensor data, we mean information that is derived solely from the VIIRS observations and geo-location information.

- Calibrated brightness temperature for channels 3.9μm, 11μm and 12μm
  - GOES-R Loop Heat Pipe mitigation - Whenever the loop heat pipe in the ABI sensor exceeds one of the channel-specific thresholds, indicating that the brightness temperature for that channel is compromised, NCOMP retrievals will produce a missing value and the Product Quality Flag will indicate bad data. For NCOMP input ABI channels, 7, 14, and 15, those thresholds are 150.0K, 150.0K, and 93.0K, respectively. Thus, when the focal plane temperature for ABI Band 15 (12μm) reached 93K, the NCOMP algorithm will not be run until returns below that threshold. This is due to the limitations of how the algorithm is performed as described in the following sections.
- Viewing zenith angle
- Solar zenith angle

3.3.2   Ancillary Data

The following briefly describes the ancillary data required to run the software to infer nighttime COD and CPS and subsequently determine LWP/IWP using the NCOMP algorithm. By ancillary data, we mean data that requires information not included in the VIIRS observations or geo-location data. Unless otherwise indicated, a more detailed description of each set of ancillary data is provided in the Algorithm Interface and Ancillary Data Description Document (AIADD). The NWP and RTM data, which are at NWP resolution, are interpolated to pixel level as described in the AIADD. While six-hour forecasts were used in the development of the ACM, and, as such, are recommended, any forecast in the 0 to 24 hour range is acceptable.

- **Surface type**

- **Surface emissivity of channels 3.9μm, 11μm and 12μm.**

- **Clear-sky infrared radiative transfer model calculations**
  Clear-sky top-of-atmosphere (TOA) radiances computed for channels 3.9μm, 11μm and 12μm. Profiles of clear-sky transmission and radiance are required for the same channels. Currently, these clear-sky temperatures and radiances, as well as the radiance and transmission profiles, are obtained by using a fast clear-sky

Radiative Transfer Model (RTM), the Pressure-layer Fast algorithm for Atmospheric Transmittance (PFAST) with 101 vertical levels that match the temperature profiles described below in the All-sky Temperature profile explanation.

- **All-sky Temperature, Height and Pressure profiles and Skin Temperature**
Knowledge of the atmospheric temperature, height and pressure profiles is required in order to place cloud temperatures at the appropriate level. Additionally, the surface skin temperature is obtained from the NWP. These are provided from the NWP as described in the AIADD.

- **Calibration Coefficients**
Due to lack of accurate calibration in some VIIRS and ABI channels and the possibility that some channels will need refined calibration during NCOMP processing, the capability to read and utilize instrument-specific calibration coefficients is included. In the 11μm brightness temperatures require recalibration, so in that circumstance a calibration is applied (see 4.2.1.3 for the rationale for channel 11μm recalibration). A simple slope and offset formulation is used and the input data file contains a description of the calibration source. These coefficients are read from the same file as the cloud emittance parameterization coefficients because those are also instrument-specific.

In the input data file two identifying text lines precede the calibration coefficients and describe the source of the coefficients, as well as the channel to which they apply. Note that when the first identifying text line uses the term "SIR", it indicates that the coefficients are for the 3.7-μm channel, aka Solar InfraRed (SIR). The slope and offset used for calibrating the SNPP SIR channel, Slope_Chn_7 and Offset_Chn_7, respectively, are contained in a third line, just after the two identifying lines. The "_7" suffix in the slope and offset variable names is used because the SEVIRI SIR data are proxies for ABI channel 7 in the GOES-R processing system, which was the model for NPSS processing.

NASA LaRC will provide calibration coefficients for additional channels and/or instruments should they be deemed necessary.

- **Cloud Emittance Parameterization Coefficients**
The retrieval uses a set of coefficients that allows the invocation of a parameterization that computes cloud effective emittances for a set of 16 cloud particle size models, both water and ice, as a function of viewing zenith angle, clear-sky temperature, and cloud temperature for each of the 3 channels currently used (Minnis et al. 1998). These parameterizations, detailed in 3.4.2.1, have been calculated for a fixed set of 8 cloud optical depth bins and the resultant cloud emittances are used in the algorithm for computing cloud temperatures in channels 3.9μm, 11μm and 12μm for each pixel. For a given channel, each of the 8 COD bins and each CPS model, 30 coefficients are contained in the file, hence the file contains 240 coefficients per channel for each of the 7 water droplet and 9

ice crystal models, i.e., 3840 coefficients per channel. The coefficients are in theory instrument-specific, but the same set of coefficients can usually be used for instruments with similar spectral responses in a given channel. These coefficients are read from the same file as the calibration coefficients because those are also instrument-specific. NASA LaRC will provide cloud emittance parameterization coefficients for additional instruments should they be deemed necessary.

The fourth line of the input data file (see Calibration Coefficients above for the description of earlier lines) contains identifying text for the emittance parameterization coefficients that includes the satellite name and the wavelength/channel to which the first set of 3840 coeffcents applies. The coefficient sets follow their corresponding identifying text line and are stored in order of increasing VIIRS channel number, so the first text line and the subsequent coefficients are for channel 3.9μm. Following the first set of 3840 coefficients another identifying text line is present for channel 11μm, followed by its set of 3840 coefficients and the file concludes with the channel 12μm identifying text line and its coefficients.

As with the calibration coefficients, the input file's identifying text line for channel 3.9μm, uses the term "SIR" which indicates the coefficients are for the VIIRS 3.7-μm channel, aka Solar InfraRed, while "IR" and "S-W" indicate the 10.76- and 12.01-μm channels, respectively, aka Infrared and Split-Window. These terms, along with the suffixes "_a", "_b" and "_c" in the coefficient variable names, all refer the 3.9μm, 11μm and 12μm, respectively.

Each of those sets is dimensioned identically to the following example for Q_Coef_Chn_a, which is the variable name used for channel 3.9μm:

Q_Coef_Chn_a (Num_OD_Bins, Ndq, Num_Mdls)

where Num_OD_Bins = 8, the number of COD bins, Ndq = 30, the number of coefficients for each COD bin and each model, and Num_Mdls = 16. The models are always ordered so that the 7 water models precede the 9 ice models with each phase set appearing in the order of increasing radius (see Table 3) and the optical depth bins also increasing from the smallest to the largest nodes (see 3.4.2.1). When reading the Q_Coef_Chn_a, Q_Coef_Chn_b and Q_Coef_Chn_c elements from the input data file they should be read in column-major order, i.e., with the COD bin changing first and the Model bin changing last.

The usage and further discussion of the parameterization coefficients is contained in 3.4.2.1 and in Appendix 2, after the scientific basis for their form has been established in 3.4.2.1.

3.3.3 Derived Data

The following briefly describes the products from other VIIRS algorithms that the NCOMP algorithm uses as input. These data are necessary in order to run the software that calculates COD, CPS, LWP and IWP. These data are required information that is not included in the VIIRS observations or geo-location data.

- **Cloud Type**
  As described in the VIIRS Cloud Phase/Type ATBD, cloud type and phase are derived prior to the invocation of the NCOMP algorithm. Currently, rather than using the VIIRS Cloud Phase, the values for VIIRS Cloud Type are input to the NCOMP algorithm where phase is then determined internally by combining various cloud types. The VIIRS phase product is determined in a similar manner, but the NCOMP algorithm is currently using its own internal combination scheme. Neither the VIIRS cloud phase or cloud mask products are being used directly because VIIRS cloud type results provide additional information and retain flexibility for future enhancements of NCOMP. NCOMP results are not impacted by this internal combination scheme; it serves only to facilitate potential future enhancements. In addition, the internally produced cloud phase allows for processing flags to be set if NCOMP or the VIIRS Cloud Type product provides an indication that the phase might be ambiguous, e.g., for mixed, multi-layered or super-cooled cloud types. This will enhance validation studies.

- **Cloud Top Temperature**
  As described in the VIIRS Cloud Temperature/Height ATBD, cloud top temperature is derived prior to the invocation of the NCOMP algorithm.

3.4 Theoretical Description

Knowledge of the LWP and IWP for water and ice clouds, respectively, is one of the primary needs of climate and weather modelers to determine radiation budgets, develop radiative transfer techniques, and modify cloud models and parameterizations. LWP and IWP are not directly retrieved on large spatial scales given current satellite technology, but fortunately, the relatively simple relationships between COD and CPS and the liquid or ice water path allow for their calculation.

The JPSS Clouds Algorithm Working Group is using a suite of algorithms for daytime and nighttime data, exploiting the strengths of each technique in order to maximize accuracies and provide feedback opportunities between techniques that were independently developed. For NCOMP a heritage algorithm from NASA Langley, the Shortwave-infrared Infrared Split-window Technique (SIST) of Minnis et al (1995, 2009), has been chosen as it is currently being applied to a variety of satellite instruments. SIST is also one of the more robust existing algorithms because it simultaneously determines phase and cloud temperature/height as well as cloud optical and microphysical properties. The NCOMP algorithm uses differences in cloud

brightness temperature, clear-sky temperature, and spectral differences to ascertain both COD and CPS and, in turn, to calculate the LWP and IWP. For the purposes of JPSS, SIST has been adapted so that it accepts as input the cloud top temperature and cloud type that are determined in other JPSS algorithms and then calculates both COD and CPS based on those inputs. The current JPSS NCOMP algorithm is identical to that developed for application to GOES-R ABI imagery and described in Minnis and Heck (2010).

3.4.1 Physics of the Problem

Numerous techniques have been developed to retrieve cloud optical and microphysical properties from narrowband radiometer measurements onboard satellites. Many of these techniques exploit spectral differences in visible wavelengths, or wavelengths comprised of both reflected and emitted components, and, therefore, are not applicable to nighttime situations.

3.4.1.1 Thermal Radiative Transfer

A simple radiative transfer relationship that describes an emitted radiance observed by a satellite at a particular wavelength, λ, at an equivalent brightness temperature T can be approximated as

$$
B(T) = L_u\uparrow(\mu) + t_u(\mu)\left\{ \left\{ t_l\left[(1-\varepsilon_s)\left[\left(L_l\downarrow_s\right) + t_l\varepsilon_d B\left(T_{cld}\right) + t_l L_u\downarrow(1-\varepsilon_d)\right] + \varepsilon_s B\left(T_s\right)\right] + L_l\uparrow\right\}(1-\varepsilon_a) + \varepsilon(\mu)B\left(T_{cld}\right) \right\}
$$

(1)

where all variables depend on λ except μ. In (1), B is the Planck function at λ, $L_u\uparrow$ is the upwelling radiance emitted by the atmospheric layer above the cloud reaching the top of the atmosphere, T_s is the surface skin temperature, T_{cld} is the cloud temperature, $L_l\downarrow_s$ is the downwelling radiance at the surface emitted by the atmospheric layer below the cloud, $L_l\uparrow$ is the upwelling radiance emitted by the atmospheric layer below the cloud reaching cloud base, $L_u\downarrow$ is the downwelling radiance emitted by the atmospheric layer above the cloud, ε_s is the surface emissivity, $\varepsilon(\mu)$ is the effective cloud emissivity at cosine viewing zenith angle μ, ε_d is diffuse cloud emissivity estimated using the diffusivity approximation, i.e., the emissivity evaluated at $\mu = 0.6$. The cloud emissivities are functions of the cloud spectral optical depth τ_λ. The transmissivities of the atmosphere above and below the cloud are represented by t_u and t_l, respectively. If scattering is neglected, then the absorption cloud emissivity is

$$\varepsilon_a = 1 - \exp(-\tau_a / \mu) \qquad (2)$$

where the cloud absorption optical depth $\tau_a = (1 - \widetilde{\omega}_o)\tau_\lambda$ and $\widetilde{\omega}_o$ is the single scattering albedo at λ. This parameter is used to estimate ε_d. The values of ε_a and ε are generally small and differ as functions of particle size and μ. Thus, in most cases ε can substitute for ε_a. However, because ε sometimes exceeds unity, it must be reset to equal 1.0 whenever $\varepsilon > 1.0$ to avoid computing negative transmissivities.

The first term in (1) is the emission by the atmospheric layer above cloud top that reaches the TOA. The second term represents all of the radiation from the cloud top and below that reaches the TOA. All secondary reflection and transmission terms have been ignored in this formulation. Within the largest brackets are two main components. The first, within the small brackets comprises three terms, the downwelling radiation reflected by the surface, upwelling radiation emitted by the atmospheric layer below the cloud, and upwelling radiation emitted by the surface, where the albedo of the surface is estimated as $(1 - \varepsilon_s)$. Within the bold square brackets are the primary components of the downwelling radiation reflected by the surface: the emission from the atmosphere under the cloud, the downwelling emission from the cloud, and the emission from the atmospheric layer above the cloud that passes through the cloud and sub-cloud atmospheric layer to reach the surface. This last term is typically very small and can probably be neglected except for the thinnest cloud. Overall, the reflected term will contribute little to the upwelling TOA radiance except for very thin clouds and relatively small surface emissivities. So, it is usually ignored in practice. The surface emission term, second term within the thin brackets, is the major contributor to the upwelling radiance below the cloud. The third term represents the upward emission of the sub-cloud layer reaching cloud base. The second term within the largest brackets is net emission from the cloud itself.

As stated above, for a given μ, ε can substitute for ε_a and the reflected terms of (1) can be ignored in practice, so (1) reduces to

$$B(T) = L_{u\uparrow}(\mu) + t_u(\mu)\left\{\left[t_l\varepsilon_s B\left(T_s\right) + L_{l\uparrow}\right]\left(1 - \varepsilon(\mu)\right) + \varepsilon(\mu)B\left(T_{cld}\right)\right\} \qquad (3)$$

when used in NCOMP. In order to verify that the emittance of the cloud is physically realistic note that if the radiance emitted from the top of the cloud is less than or equal to 0.0 then it is assumed that it is equal to the cloud radiance itself.

For semi-transparent clouds, it is possible to estimate ε_λ and T_{cld} from simultaneous measurements at two different wavelengths λ_i and λ_j, if the clear-sky temperature at that wavelength, $T_{cs\lambda}$, and the relationship between $\varepsilon_{\lambda i}$ and $\varepsilon_{\lambda j}$ is known and $\varepsilon_{\lambda i} \neq \varepsilon_{\lambda j}$. If ε_λ is known, then τ_λ can be determined from the equation above or some other function that relates the two quantities. In JPSS applications, T_{cld} is known from other JPSS algorithms so it is theoretically possible to determine particle size, r_e, and τ_λ, assuming that the

optical properties of the clouds are different at wavelengths λ_i and λ_j. As discussed below, many techniques make use of the brightness temperature difference BTD_{i-j} between T_i and T_j to provide information about the particle size and optical depth (Note that for consistency with the published literature cloud particle size is sometimes referred to as effective radius in this ATBD).

3.4.1.2 Cloud Microphysics

Over some distance, z_1 to z_2, the spectral optical depth for a given size distribution can be determined from

$$\tau_\lambda = \pi Q_e \int_{z_1}^{z_2} N r_e^2 dz \qquad (4)$$

where Q_e is the extinction efficiency and N is the total particle number density. For a water cloud, the particle size between some size distribution between r_1 and r_2 is

$$r_e = \frac{\int_{r_1}^{r_2} r \pi r^2 n(r) dr}{\int_{r_1}^{r_2} \pi r^2 n(r) dr} \qquad (5)$$

where $n(r)$ is the number density of droplets with radius r. For ice particles, using the techniques from Minnis et al. (1995) the effective diameter is

$$D_e = \frac{\int_{L_1}^{L_2} D(L) \pi A_e(L) n(L) dL}{\int_{L_1}^{L_2} \pi A_e(L) n(L) dL} \qquad (6)$$

where $D(L)$ is the volume equivalent diameter of the hexagonal ice crystal of length L and width d. A_e is the cross-sectional area where there is an assumed monotonic relationship between L and d for the hexagonal ice columns as defined in Takano and Liou (1989). The equivalent particle size can be computed from D_e using the following equation,

$$r_e = 0.4441 \, D_e + 1.0013\text{E-}3 \, D_e^2 + 7.918\text{E-}9 \, D_e^3 \qquad (7)$$

where D_e has been defined for the particle size distributions given by Minnis et al. (1998). The LWP or IWP is computed as a function of τ and r_e as explained in section 3.4.2.2.

Thermal-only techniques that are applicable during either day or night are typically based on BTDs between two or more thermal channels, e.g., Inoue (1985), Ackerman et al. (1990), Lin and Coakley (1993), Baum et al. (1994), Minnis et al. (1995, 2011), Fu and Sun (2001), Katagiri and Nakajima (2004), and Chiriaco et al. (2004). While each of

these algorithms and their variations are capable of deriving COD and CPS, some also simultaneously determine cloud temperature, height and other interdependent quantities, but most assume a priori knowledge of either the cloud height and/or thermodynamic phase.

These methods ultimately rely on the differences in the imaginary indices of refraction (IIR) among the various channels. Figure 2 plots the IIRs for liquid and ice water from Downing and Williams (1975) and Warren (1984) for part of the relevant spectral range. Both the 11- and 12-µm channel ice IIRs are twice their respective water values. However, the difference between the 11- and 12-µm ice IIRs is double the difference between their water counterparts. For the 8.5-µm channel, the IIRs are the same for ice and water, while the ice and water IIRs for the 3.9-µm channel (not shown) are roughly 5% of the values for the 11-µm channel. These differences in IIR among the
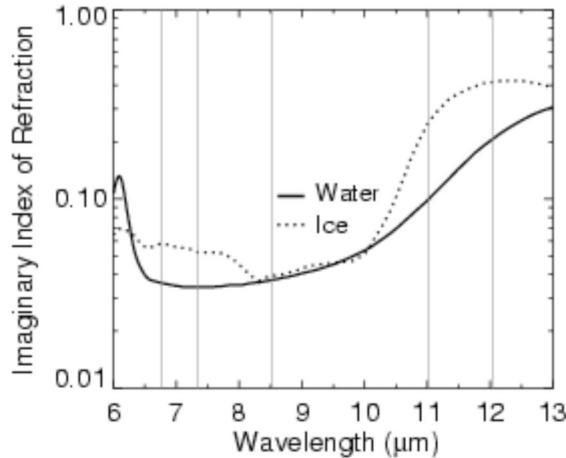
Figure 2. Imaginary indices of refraction for part of the infrared spectrum.

channels translate to differences in absorption as represented by the single scattering albedo computed via Mie scattering theory for water droplets or, for ice crystals, via geometric optics or some other technique. As radius increases, both the path length through the particle and $\tilde{\omega}_O$ increase for strongly absorbing wavelengths such as those in Fig. 2. For weakly absorbing wavelengths (e.g., 3.9 µm), $\tilde{\omega}_O$ decreases with increasing radius (e.g., Minnis et al., 1998). For both absorption types, $\tilde{\omega}_O$ approaches 0.5 because the diffraction takes out about half of the energy available for absorption. Because of these spectral absorption differences, the BTD between a given pair of channels will depend on the particle size, optical depth, and difference between the surface and cloud temperatures.

The reference wavelength for most cloud retrievals is the 0.64-µm or VIS channel. The spectral optical depth is related to the VIS optical depth through the extinction efficiencies,

$$\tau_\lambda = \tau_{VIS} \, Q_\lambda / Q_{VIS}. \tag{8}$$

For smaller particles, Q_λ ranges from 0.3 to 1.9 at longer wavelengths. For larger particles Q_λ varies from 1.9 to 2.2, while it is typically between 2.0 and 2.6 for 3.9 and the VIS wavelengths (e.g., Minnis et al., 1998). Given (2) and (8), the emittances for larger particles are ~0.95 and 0.982 for τ_{VIS} = 6 and 8, respectively, at a nadir view for both 11 and 12 μm. Thus, the $BTD_{11\text{-}12}$ approach zero for optical depths τ_{VIS} > ~6. Since most geostationary satellite observations are taken off nadir, the limiting optical depths will typically be much smaller (~3 for μ = 0.5). For smaller particles, the limiting optical depths can be somewhat smaller. Thus, the SIST-type retrievals are constrained mostly to semi-transparent clouds. This limits the amount of information that can be retrieved compared to daytime when the use of solar reflectance yields optical depths exceeding 100.

The theoretical curves in Figure 3, reproduced from Minnis et al. (1998) show the typical behavior of the BTDs as functions of particle size and phase for a cloud temperature of 260 K for AVHRR channels, but the situation is analogous for NPP VIIRS and VIIRS channels. That is, $BTD_{3.75\text{-}10.8}$ tends to decrease with increasing particle size for ice clouds (Fig. 3a) and vice versa for water clouds (Fig. 3b). However, $BTD_{11\text{-}12}$ decreases with increasing particle size for both water and ice (Figs. 3c,d). The BTD values are also dependent on the difference between T_{cld} and T_{cs} because they constrain the maximum

24
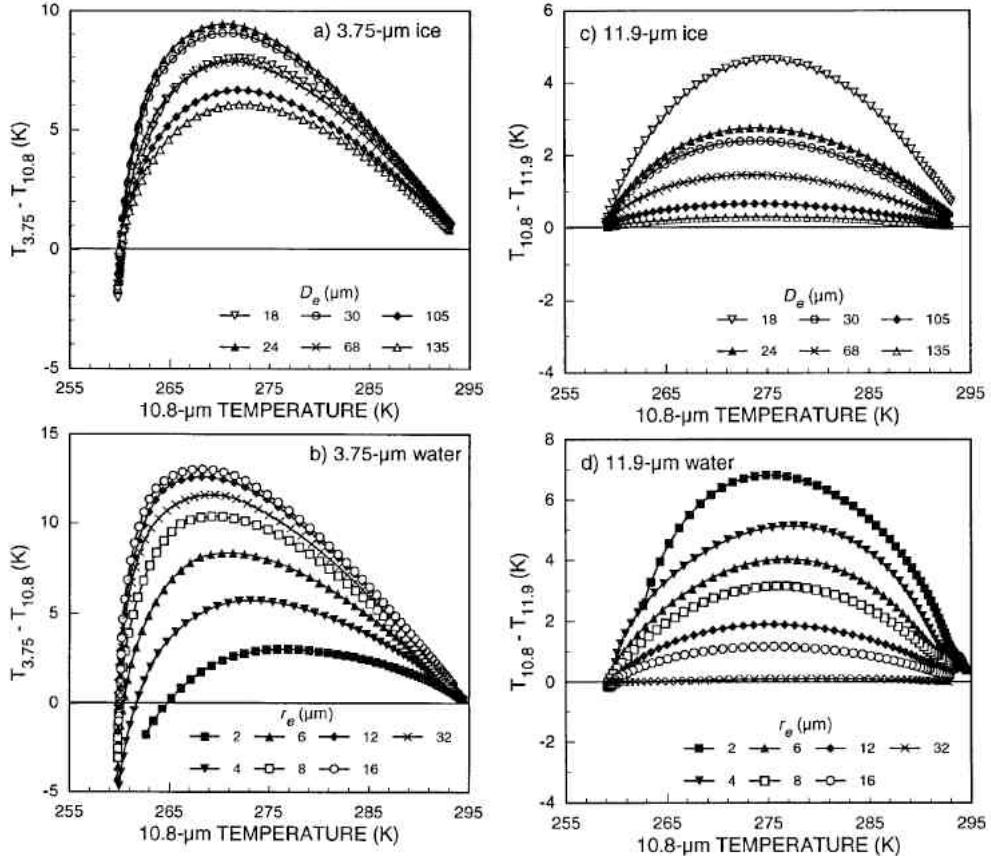
Figure 3. Modeled BTDs from the emittance parameterizations for clouds of various r_e and D_e for T_{cs} = 295, T_{cld} = 260 K, τ = 16 and viewing zenith angle = 30°.

values. Thus, usable information is available over a greater range of τ_{VIS} for a greater contrast between the surface and cloud temperatures. As T_{cld} approaches T_{cs}, the utility of the SIST diminishes, but not entirely since $BTD_{3.75-10.8}$ tends toward some negative limiting value because of scattering at 3.75 µm.

Discussion of the particle size limits that can be retrieved using these techniques can be found in Lin and Coakley (1993).

3.4.2 Mathematical Description

NCOMP determines the cloud optical depth and cloud particle size that produce modeled brightness temperatures that are closest to the observed brightness temperatures for each SNPP VIIRS proxy pixel. Observed BTDs are compared to modeled, i.e., simulated, BTDs and cloud physical parameters are inverted. The effective radius, r_e, and τ that produce the minimum difference between observed and modeled BTDs for each pixel are assumed to describe the cloud. The phase-appropriate water path, either LWP or IWP, is calculated based on the retrieved r_e and τ.

3.4.2.1 Emittance Parameterizations

Similar to the methods of Minnis et al. (1998), the cloud emittance models used by NCOMP comprise a set of coefficients that were calculated for the MODIS 3.7-µm channel and the GOES 10.8- and 12-µm channels. While the MODIS and GOES channel characteristics vary from the analogous VIIRS channels, the quality of the retrieved parameters is thought to be sufficient for the purposes of testing NCOMP using SNPP VIIRS data. The effective emittance, which includes the effects of both scattering and absorption, is used instead of the absorption emittance to maximize the accuracy of the simulated radiances. For each set of water droplet and ice crystal models and for the aforementioned wavelengths, the following regression formula was fitted to effective emittances computed using radiances calculated with the adding-doubling radiative transfer model of Minnis et al. (1993):

$$\varepsilon_\lambda(\zeta,\mu,\xi) = \sum_{i=0}^{2} \sum_{j=0}^{4} \sum_{k=0}^{1} d_{ijk} \zeta^i \mu^j \xi^k$$

(9)

where ζ = 1/ln(ΔT_{sc}), ΔT_{sc} = T_{cs} − T_{cld}, ξ = 1/ln(T_{cs}) and μ is the cosine viewing zenith angle. The clear sky temperature, T_{cs}, is equivalent to $\varepsilon_{s\lambda}B_\lambda(T_s)$ in the thermal radiative transfer equation and includes atmospheric attenuation because it is a TOA quantity, i.e., T_{cs} is the upwelling brightness temperature at the bottom of the cloud. A set of coefficients, d_{ijk}, was determined for each optical depth node and particle size model, ice

and water, where i, j, and k are the exponents for ζ, μ and ξ, respectively. These coefficients and the order of the exponents were determined by minimizing the squared error in the regression analyses, which generated eight sets of 30 coefficients for each microphysical model and spectral band. The complexity of (9), as compared to (2), is necessary because (2) cannot account for scattering by the cloud particles. The parameterizations were developed for 7 water droplet models using Mie scattering theory and 9 ice crystal size distributions using hexagonal columns and ray-tracing to obtain optical properties. The particle size models and their respective cloud particle sizes are detailed in Table 3. The calculations were performed for 8 nodes of visible τ (0.25, 0.5, 1.0, 2.0, 4.0, 8.0, 16.0 and 32.0) and for realistic ranges of T_{cs} and T_{cld}. Note that the emittance parameterizations and their subsequent usage in NCOMP allow the direct retrieval of τ_{VIS}, i.e., COD, in Equation (8). There is no conversion from τ_λ to τ_{VIS} necessary due to NCOMP's advantageous usage of differences

Table 3. Water and ice crystal particle size models used in emittance parameterization.

Effective Radius/Diameter	Phase
r_e = 2, 4, 6, 8, 12, 16 and 32 μm	water
D_e = 5.83, 18.15, 23.86, 30.36, 45.30, 67.60, 104.9, 123.0, and 134.9 μm	ice

between T_{cs} and T_{cld}, as detailed in Minnis et al. (1998). In general, however, the ratio of τ_{VIS} to infrared optical depth ranges from 2.0 for the largest particles to ~2.5 for the smallest ice crystals and up to ~4 for the smallest water droplets.

The mean rms errors of ε_λ from (9) are less than 0.001 and 0.002 for λ = 12 and 11 μm, respectively, compared to the complete adding-doubling calculations. For λ = 3.9 μm, the rms errors range from 0.003 for the largest water droplets to 0.02 for the r_e = 2 μm, and from < 0.001 for large ice crystals to 0.005 for the D_e = 5.83 μm. The parameterized emittances yield uncertainties in simulated brightness temperatures of ~0.05 K for 11- and 12-μm channels and ~0.5 K at 3.9 μm for most conditions. More information about the parameterizations and adding-doubling calculations can be found in Minnis et al. (1998). The parameterizations can be created for other instruments and wavelengths and, if deemed necessary, will be provided by NASA Langley.

3.4.2.2 Retrieval Technique

The NCOMP algorithm utilizes the parameterizations of effective emittance in an iterative scheme that minimizes the BTDs between the computed and observed temperatures at 3.7, 10.8 and 12.0 μm. For each VIIRS pixel for which a valid Cloud Type, i.e., Cloud Type is neither clear nor unknown, and a valid T_{cld}, i.e., $T_{cld} > 0.0$, have been provided, the emittance parameterization is first used to compute $\varepsilon_{10.8}$ for each phase-appropriate particle size model using ΔT as computed from the input T_{cs} and T_{cld}.

As described in 3.3.3 and as shown in Table 4, the phase is determined by collapsing the VIIRS Cloud Type into NCOMP phase categories. Note that Cloud Types of Spare and Overshooting Top are not yet implemented in the Cloud Type Algorithm, however, since NCOMP is insensitive to the numerical value of Cloud Type, NCOMP can check the static global structure for those Cloud Types. This will allow usage of these Cloud Types should the become available in the future with the added benefit of not requiring code changes. In the iteration initialization step for each particle size model, a first guess

Table 4. Assignment of cloud phase from VIIRS Cloud Type in NCOMP.

VIIRS Cloud Type and Value	NCOMP Phase
Clear	no analysis
Spare*	water
Water	water
Supercooled	water
Mixed	water
Tice	ice
Cirrus	ice
Overlap	ice
Overshooting Top*	ice
Unknown	no analysis

*Future Cloud Type values

determination of $\varepsilon_{10.8}$ is made with τ assumed to be 1.0 and an initial estimate of the modeled brightness temperature, $T'_{10.8}$, is produced using Equation (3) with the appropriate above- and below-cloud atmospheric transmittances from the RTM, as well as T_s and T_{cld}. An iterative scheme then commences by adding 0.1 to τ, computing a new $T'_{10.8}$ and the accompanying differences between the two $T'_{10.8}$ guesses and the observed temperature $T_{10.8}$. After these first two guesses are made, the scheme iterates in τ by continuously updating τ weighted by the ratio of the τ differences to the corresponding temperature differences, hence for each iteration, m, the subsequent guess $\tau_{m\square\square}$ is

$$\tau_{m\square\square} = \tau_\square + (T'_{10.8,m} - T_{10.8})(\tau_{\square-\square} - \tau_\square) / [(T'_{10.8,m} - T_{10.8}) - (T'_{10.8,m-1} - T_{10.8})]. \qquad (10)$$

After $\tau_{m\square\square}$ is calculated in Equation 10, in the unlikely situation that $\tau_{m\square\square}$ is less than or equal to 0.0, it is set to 0.01.

The iteration continues either (1) until the newly calculated BTD, i.e., the difference between $T'_{10.8}$ calculated by the forward model with τ_m and the observed $T_{10.8}$, is equal to the difference between the previously calculated BTD (the difference between $T'_{10.8}$ calculated by the forward model with τ_{m-1} and the observed $T_{10.8}$), (2) until the number of iterations is greater than or equal to 15, or (3) until the difference between $T'_{10.8}$ calculated with τ_m and the observed $T_{10.8}$ is less than or equal to 0.01. Any of those three

exit conditions can cause the iteration to end. Condition (1) is evaluated just prior to the computation of $\tau_{m\square\square}$ using Equation 10, while conditions (2) and (3) are evaluated as the last step of each iteration. Additionally, once the iteration has been exited, τ is set to the minimum of 16.0 and the τ value from the iteration.

The fact that the computation of $\tau_{m\square\square}$ takes place after testing for condition (1), hence after the evaluation of Equation 3 using τ_m, results in two possible scenarios for τ being set upon exiting the iteration. The first scenario, when condition (1) is true, results in $\tau = \tau_m$, while the second scenario, when either condition (2) or (3) is true, results in $\tau = \tau_{m\square\square}$. The impact on τ of these two different paths is minimal due to the small changes in τ as convergence is approached. At this point each τ has been determined for each cloud particle size model as this procedure has been invoked for each of the 7 water or 9 ice models.

Note that whenever atmospheric transmittances or radiances are used in the calculations, they are obtained using the appropriate levels of the RTM profiles. The AIDDD-described routine Prof_Lookup_Using_Z is used to determine which RTM and NWP profile level contains T_{cld}. The cloud is assumed to be at the bottom of the layer defined by the level determined by Prof_Lookup_Using_Z and the level vertically beneath that level, hence, for indexing purposes the level beneath that returned by Prof_Lookup_Using_Z is considered the cloud level. Computations of below cloud quantities do not include the cloud level whereas computations of above cloud quantities do. Additionally, the fast Planck function, also detailed in the AIADD, is used to convert temperature to radiance and vice versa.

Note that in the above scheme whenever $\varepsilon_{10.8}$ is needed when calculating $T'_{10.8}$ for a particular combination of T_s, T_{cld}, $T_{10.8}$, τ and r_e for a cloud particle size model, it is necessary to interpolate between the optical depth nodes of the emittance parameterization. NCOMP utilizes a standard Lagrangian N-point interpolation scheme of emittance on natural log of τ using the parameterization τ nodes of 0.25, 0.5, 1.0, 2.0, 4.0, 8.0, 16.0 and 32.0. This interpolation scheme is described in Appendices 1.1 through 1.3.

The τ calculated as above for each of the phase-appropriate models is then used to calculate the simulated temperatures for the other two NCOMP channels, $T'_{3.7}$ and $T'_{12.0}$. For both 3.7 and 12.0 μm, the emittance parameterization is invoked again, although for these channels τ has already been determined so no iteration in τ is needed. While the $T'_{3.7}$ and $T'_{12.0}$ calculations are analogous to the $T'_{10.8}$ calculations, those for $T'_{3.7}$ include a variation of the Lagrangian N-point interpolation scheme, also described in Appendix 1 and particularly in Appendix 1.4, that addresses a different functionality for $\tau > 4.0$ at 3.7 μm. Still using natural log of τ, this variation interpolates in temperature rather than emittance, but results in $\varepsilon_{3.7}$ and $T'_{3.7}$, just as with the other λ. At this point then, for each particle size model τ is set as are $T'_{3.7}$, $T'_{10.8}$ and $T'_{12.0}$, each with its appropriate $\varepsilon_{3.7}$, $\varepsilon_{10.8}$ and $\varepsilon_{12.0}$, but these solutions are only for the r_e of the 7 water models if the inferred phase was water or, conversely, the 9 ice models if ice. An error for each of the models

$$E(r_e) = [(T'_{3.7} - T'_{10.8}) - (T_{3.7} - T_{10.8})]^2 + [(T'_{10.8} - T'_{12.0}) - (T_{10.8} - T_{12.0})]^2 \quad (11)$$

is computed from the BTDs in order to determine which model with its corresponding τ and ε best describes the observed brightness temperatures, i.e., has the smallest $E(r_e)$.

Once this minimum error model n with its associated r_e is identified, an interpolation scheme that utilizes the same iterative τ determination method as above is invoked to interpolate between adjacent models and their τ nodes which allows for the computation of off-node τ values and pinpointing of the actual r_e that is likely to lie between adjacent particle size models. Note that for both water and ice, models are always ordered by increasing r_e. First, a model-dependent particle size step is chosen from Table 5 that is used to reduce $r_e(n)$, the r_e for model n, and calculate a new solution between particle size

Table 5. Particle Size steps for interpolating between particle size models.

Model Effective Radius/Diameter	Phase	Particle Size Step
2 to 16 μm	water	0.10
16 to 32 μm	water	0.20
5.83 to 18.15	ice	0.10
18.15 to 123.0 μm	ice	0.20
123.0 to 134.9 μm	ice	0.50

models n and $n-1$. The first calculation away from n is for $r_e(n)$ reduced by the step value and a new error is recomputed using Equation (11). The same procedure is repeated between models n and $n+1$ with $r_e(n)$ increased by the step, resulting in the computation of a high side error. It is assumed that the side of model n with the lowest error will contain the ultimate solution, so the two $E(r_e)$ on either side of model n are compared to each other, hence determining the side that contains the solution. Additionally, it is assumed that $E(r_e)$ is always either monotonically increasing or decreasing with r_e as steps are taken away from the minimum error model. If neither of the low or high side steps away from the minimum error model is larger, then CPS becomes the model value

When decreasing r_e from the particle size associated with model n, a new τ is necessarily calculated with each computation of $E(r_e)$, iterating to obtain τ as discussed earlier, but now linearly interpolating between $\varepsilon_{10.8}(n)$ and $\varepsilon_{10.8}(n-1)$ based on the appropriate step (still from Table 5) divided by $r_e(n) - r_e(n-1)$. This weighted $\varepsilon_{10.8}$ is in turn used to compute a weighted $T'_{10.8}$ using Equation (1). Similarly, during each step away from $r_e(n)$ when $T'_{3.7}$ and $T'_{12.0}$ are computed for usage in Equation (10), $\varepsilon_{3.7}$ and $\varepsilon_{12.0}$ use the same linear weighting scheme. Step calculations when increasing r_e use this same process, but the linear interpolation uses the appropriate step divided by $r_e(n+1) - r_e(n)$.

Once it is known which of the low or high sides of model n contains the best solution, the technique focuses on the low error side and successively decreases or increases r_e by the same step factor until a minimum $E(r_e)$ is reached. When that minimum is reached, the corresponding τ and r_e are declared the best possible solution. Note that a solution is chosen when either the error minimizes or when 99% of $r_e(n+1)$ - $r_e(n)$ has been traversed for the high side computations or, on the low side, when 99% of $r_e(n)$ - $r_e(n-1)$ has been traversed.

If the smallest phase-appropriate particle size model is associated with the smallest error, i.e., $n=1$, then it is not necessary to compute both a low side and high side error. Only the $E(r_e)$ for successive steps increasing from $r_e(n)$ are calculated and a solution is chosen when the error minimizes or when 99% of $r_e(n+1)$ - $r_e(n)$ has been traversed. Likewise, when the largest phase-appropriate model is associated with the smallest error, the $E(r_e)$ for successive steps decreasing from the largest model's particle size are calculated and a solution is chosen when the error minimizes or when 99% of $r_e(n)$ - $r_e(n-1)$ has been traversed.

Because of the need to conduct multiple iterative steps when interpolating between models and model nodes, the emittance parameterization is invoked numerous times reinforcing the need for not including explicit radiative transfer steps in the retrieval scheme. An additional time-saving measure is utilized whenever the parameterization of emittance is invoked for a particular pixel. Since ε_λ in Equation (9) is a function of ζ, ξ and μ, whenever a new value of either of those quantities is encountered in the iteration process, the corresponding contribution from coefficients d_{ijk}, ζ, ξ and/or μ need to be recomputed to obtain the emittance for the eight optical depth nodes and the phase-appropriate CPS model. If, however, not all of those values of ζ, ξ and μ have changed in successive computations of emittance, then only the appropriate components of Eq. 9 need to change. The application of this technique and the method of evaluating Equation (9) are detailed in Appendix 2. While Equation 9 could be explicitly evaluated for each computation of cloud emissivity, it is more efficient to use the technique in Appendix 2.

The phase-appropriate water path, either LWP or IWP, is calculated based on the final values of the retrieved r_e and τ with methods that are similar to those described by Minnis et al. (1998). For water the extinction efficiency, Q_e, is computed from a simple quadratic parameterization in the form

$$Q_e = a_0 + a_1 \ln(r_e) + a_3 [\ln(r_e)]^2 \tag{12}$$

where $a_0 = 2.416$, $a_1 = -0.1854$ and $a_3 = 0.0209$. The LWP is then obtained with

$$LWP = \frac{4}{3Q_e} \tau r_e. \tag{13}$$

For ice, another parameterization yields

$$IWP = \tau \left[b_0 D_e + b_1 (D_e)^2 + b_3 (D_e)^3 \right] \qquad (14)$$

where $b_0 = 0.259$, $b_1 = 0.000819$ and $b_3 = -0.00000088$.

Note that accurate NCOMP retrievals of τ and r_e are not possible for optically thicker clouds, as detailed in 3.4.1.2, and that retrievals for overlapped clouds will be less certain than those for single layer clouds due to the assumption that the observed radiance of a cloudy pixel is emitted from a single-layer cloud. Although the GOES-R NCOMP F&PS requirements apply only for single layer clouds with $1 \leq COD \leq 5$, NCOMP does provide qualitative retrievals of COD, CPS, LWP and/or IWP for situations when COD is less than or equal to 16. While retrievals in these are not likely to be reliable, we have included them so that further validation studies of these more difficult cases and potential algorithm enhancements can continue. For NCOMP, if the retrieved COD is greater than 16, then COD is set to 16 and the remaining parameters are retrieved as if COD was equal to16.

The capability to use default particles sizes and optical depths in the case of optically thick clouds, i.e., when COD > 5, is also included, but not utilized in the 100% code delivery. This capability could be controlled by a configuration parameter that has yet to be included in NCOMP, but could be added easily. The selection criteria for the default COD and CPS are given by Minnis et al. (2009) with values ranging from $\tau =8$, 16, or 32, r_e = 6, 8, or 10 µm, and D_e = 24 or 64 µm, depending on surface type and cloud temperature. These will be fully discussed should the range of COD of the quantitative retrievals for clouds with $1 \leq COD \leq 5$ need to be expanded in the future. NCOMP retains Surface Type as an input parameter for this purpose because the default COD and CPS values for are a function of Surface Type, reflecting the dependence of cloud characteristics on the underlying surface.

Another yet to be included configuration parameter could also control the process of overriding of the input skin temperature utilized by NCOMP. While a processing flag (see 3.4.3.2) does report the results of this process, a configuration parameter could allow this scheme to be passed over should the differences between the input skin temperature and NCOMP-calculated skin temperature be rectified in the future. Note that the value of T_s is crucial because it, along with ε_s, is used in Equation (3) for each channel to calculate the upwelling radiance from the underlying surface. Currently, for each pixel a first guess of T_s is obtained from the NWP data set. In an attempt to verify the accuracy of this value, a second value of T_s is calculated by moving the VIIRS clear sky TOA radiance at 10.8 μm to the surface and accounting for both the atmospheric radiance and transmittance, obtained from the RTM profiles of each, as well as the surface emissivity. The resultant radiance is converted to temperature using the fast Planck function and compared to T_s. If the absolute difference between these two values of T_s is > 0.1º(K), then the original NWP-based value is assumed to be more accurate and is used for the remainder of NCOMP and the processing flag in 3.4.3.2 is set to 1. In the development of NCOMP for GOES-R purposes, large differences between these two values of skin temperature were noted, hence the capability to assess the differences between these two values was included. At this time, it is not certain that either value is intrinsically

superior, but first estimates indicated that the NWP T_s was reasonable. Given that there is the possibility that either version of T_s could become more accurate or the atmospheric profiles of radiance and/or transmittance could change, it is preferred to input all channels' TOA clear sky radiances should they be needed in the future.

Whenever a clear sky temperature calculation is required for a particular point in the atmosphere, e.g., the temperature corresponding to the below-cloud radiance in Eq. 3, i.e., $t_l \varepsilon_s B(T_s) + L_{l\uparrow}$, the atmospheric transmittance and the upwelling atmospheric radiance are obtained from the RTM profile. The RTM atmospheric radiation profile passed to NCOMP arrives cumulative downward, hence to obtain the below-cloud radiation, the profile's value at the cloud level simply needs to be subtracted from the profile's value at the surface. As previously noted, the cloud is assumed to reside in the layer between the bottom of the layer defined by the level determined by Prof_Lookup_Using_Z and the level vertically beneath that level.

Similarly, the RTM profile of transmittance is stored cumulative downward. Instead, transmittance above the cloud must be removed. Unlike the atmospheric radiation, to find the below cloud atmospheric transmittance, however, the transmittance in the cloud layer and above is removed from the total atmospheric transmittance (obtained from the surface value) is divided by the transmittance at and vertically above the cloud layer.

Analogously, when a skin temperature calculation is required, as in the aforementioned method of evaluating the relative accuracies of the NWP-provided T_s and the value of T_s calculated from the VIIRS TOA clear sky radiance, L_{TOA}, the profile is used and accessed in a similar manner. The derivation of T_s from L_{TOA} requires "moving" that quantity to the surface. Fortunately, the impact of a cloud does not need to be considered as this is a clear sky calculation, so the total atmospheric radiance, L_{atm}, and total atmospheric transmittance, t_{atm}, is all that is needed to account for the atmosphere. Those quantites, as previously mentioned, are obtained from the radiance and transmittance profiles at the surface level since they are stored cumulative downward. So, instead of "adding" the atmospheric effects as in the computation of below-cloud radiance, this computation "removes" the impact of the atmosphere to obtain quantities at the surface. In other words, the calculated T_s is $B^{-1} \{[(L_{TOA} - L_{atm}) / t_{atm}] / \varepsilon_s\}$ where B^{-1} is the inverse planck function.

As mentioned in 2.1, NCOMP is responsible for calculating COD, CPS, LWP and IWP at night and when $82^o <$ solar zenith angle and $< 90^o$, but for the latter in a qualitative sense only. In twilight conditions the same technique as described above is utilized, but at its current level of maturity, only the 10.8- and 12.0-μm VIIRS channels are used due to the complicating factor of modeling the reflected solar radiation in the 3.7 μm measurements. The computations and logic are all identical, but Equation (11) reduces to

$$E(r_e) = [(T'_{10.8} - T'_{12.0}) - (T_{10.8} - T_{12.0})]^2 \qquad (15)$$

and all calculations related to the 3.7-μm channel are eliminated. NASA Langley does employ the 3-channel technique for twilight angles in its operational and research

retrievals, but in the GOES-R framework the additional overhead and coding intricacies attributable to including look-up tables for simulating the reflected portion of the 3.7 µm radiances was judged to be unnecessary for qualitative-only results. Should the GOES-R AIT desire quantitative results during twilight in the future, NASA Langley can provide these items, hence increasing the accuracy of twilight NCOMP retrievals.

3.4.3 Algorithm Output

3.4.3.1 Algorithm Products

The output of the NCOMP provides the following VIIRS cloud products:

- Visible Cloud Optical Depth (dimensionless)
- Cloud Particle Size (μm)
- Liquid Water Path (gm^{-2})
- Ice Water Path (gm^{-2})

All of these products are derived at the pixel level for all cloudy pixels with valid retrievals of cloud type and cloud temperature. The Full Disk Cloud Liquid Water Path product has a Mode 3 30 minute refresh, the Cloud Particle Size Distribution has a Mode 4 Full Disk 15 minute refresh, and the Cloud Optical Depth has a Mode 3 CONUS 15 minute refresh, therefore they should be run once every 30 minutes, 15 minutes and 15 minutes, respectively. To create the Cloud Optical Depth 4 km Full Disk Product, the Cloud Optical Depth good quality pixels will be averaged over a 2 x 2 block of pixels.

Note that COD is a dimensionless quantity that is a function of the cloud geometric thickness, liquid or ice water content and the size distribution of the water droplets or ice crystals. COD is not equivalent to geometric thickness of cloud and has no units.

3.4.3.2 Product Processing Flags

The NCOMP product processing flags are described in more detail in section 5.3. A list of the product processing flags is provided in Table 6.

Table 6. NCOMP Processing Flags.

Bit	Processing flag name	Cause & Effect
Valid Retrieval Flags		
1	QC_SZA_TWILIGHT_	82.0º <= Solar Zenith Angle < 90.0º
2	QC_CTWATER_NCOMPICE	Cloud Type = water, NCOMP preferred phase = ice
3	QC_CTICE_NCOMPWATER	Cloud Type = ice, NCOMP preferred phase = water

4	QC_CTMIX_NCOMPWATER	Cloud Type = mixed, NCOMP preferred phase = water
5	QC_CTMIX_NCOMPICE	Cloud Type = mixed, NCOMP preferred phase = ice
6	QC_CTSC_NCOMPWATER	Cloud Type = supercooled, NCOMP preferred phase = water
7	QC_CTSC_NCOMPICE	Cloud Type = supercooled, NCOMP preferred phase = ice
8	QC_CTOL_NCOMPWATER	Cloud Type = overlap, NCOMP preferred phase = water
9	QC_CTOL_NCOMPICE	Cloud Type = overlap, NCOMP preferred phase = ice
10	QC_MINERR_WATER_1	Minimum error model for water = 1
11	QC_MINERR_ICE_1	Minimum error model for ice = 1
12	QC_MINERR_WATER_LAST	Minimum error model or water = largest
13	QC_MINERR_ICE_LAST	Minimum error model for ice = largest
14	QC_TSURF_CHANGE	Skin Temperature from NWP used rather than from input

3.4.3.3 Product Quality Flags

The NCOMP product processing quality is described in more detail in section 5.3. A list of the product quality flags is provided in Table 7.

Table 7. NCOMP Quality Flags.

Value	Quality flag name	Cause & Effect
Successful Retrieval Flag		
0	QC__GOOD	Successful retrieval
Angle Restriction Flags		
1	QC_CYCLE_VZA	Viewing Zenith Angle >= 65.0º or Not Good Retrieval
2	QC_CYCLE_SZA	Solar Zenith Angle < 82.0º
Ancillary Data Flags		
3	QC_CYCLE_NOCLOUD	Cloud Type indicates it is not a cloud
4	QC_CYCLE_CLOUDTYPE	Cloud Type has an unknown value
5	QC_CYCLE_TCLOUD	Cloud Temperature is < 0.0 (C)
No Retrieval Flags		

6	QC_MINERR_WATER_0	No retrieval: Minimum error model for water = 0
7	QC_MINERR_ICE_0	No retrieval: Minimum error model for ice = 0

3.4.3.4 Product Metadata

In addition to the common metadata prescribed in the JPSS AIADD, The output files will include the following metadata specific to the NCOMP algorithm:

- Day/Night flag
- Mean, Min, Max and standard deviation of cloud optical depth
- Mean, Min, Max and standard deviation of cloud particle size
- Number of QA flag values
- For each QA flag value, the following information is required:
  - Number of retrievals with the QA flag value
  - Definition of QA flag
- Total number of detected cloud pixels
- Terminator mark or determination

4 TEST DATA SETS AND OUTPUTS

4.1 Simulated Input Data Sets

As described below, the proxy data set used to test the NCOMP is comprised of NPP VIIRS observations. The time periods chosen consisted of a 2.5 month data set including imagery from April 2014, July 2014, October 2014 and January 2015, thereby accounting for seasonal variations. The analysis spans the entire NPP VIIRS domain and should therefore encompass a full range of conditions.

4.1.1 NPP VIIRS Data

NPP VIIRS provides 22 spectral channels with a spatial resolutions ranging from 750m to 750m. NPP VIIRS currently represents the best source of data for testing and developing the NCOMP. Figure 4 is a NPP VIIRS 10.8-µm image from a test case on ??. The NPP VIIRS data were provided by the SSEC Data Center.

FIGURE 4 is missing and will be included in the next delivery

or sent separately in early January 2016, whichever is preferred.

Figure 4. Full disk 10.8-µm grayscale image from NPP VIIRS for ??. It should the same as the VIIRS 10.8-µm channel.

4.1.2 VIIRS-Derived Inputs

In addition to the image spectral radiances, inputs from other VIIRS products, in particular, T_{cld} and Cloud Type, are needed to execute NCOMP. Figures 5 and 6 show the values of T_{cld} and Cloud Type, respectively, for the test case of 0059 UTC, 17 July 2014. These VIIRS-derived products along with the $\varepsilon_{s\lambda}$, and T_s, surface type, and profiles of spectral atmospheric transmissivities and temperatures are then used to compute the modeled top-of-atmospheric brightness temperatures as in Equation (1). The results are then used to solve for r_e and τ. Note that the Cloud Type product is combined internally in NCOMP to produce an NCOMP version of cloud phase, as detailed in 3.3.3 and in Table 4.
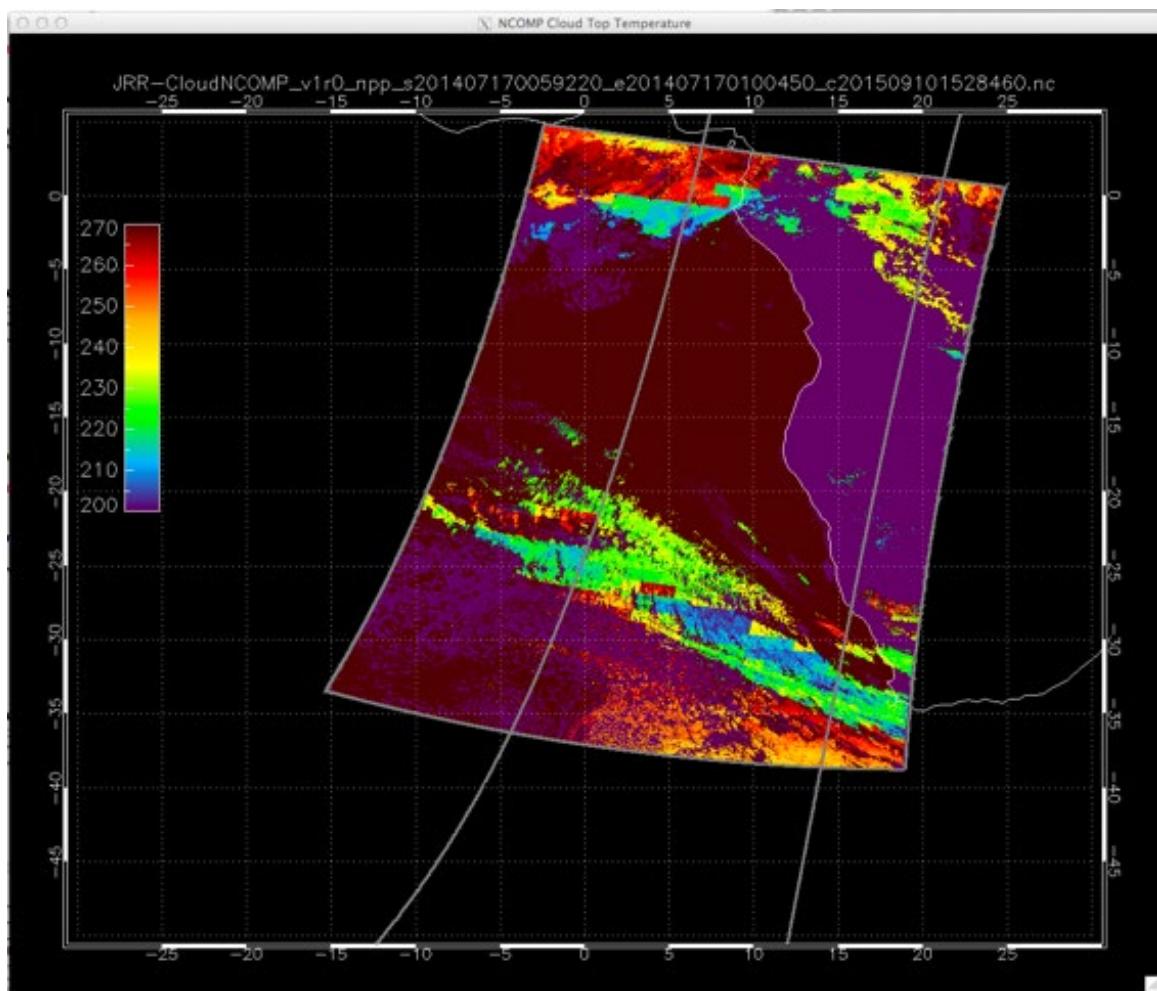
Figure 5. T_{cld} (K) input from VIIRS Cloud Height/Temperature algorithm for ~0059 UTC, 17 July 2014.
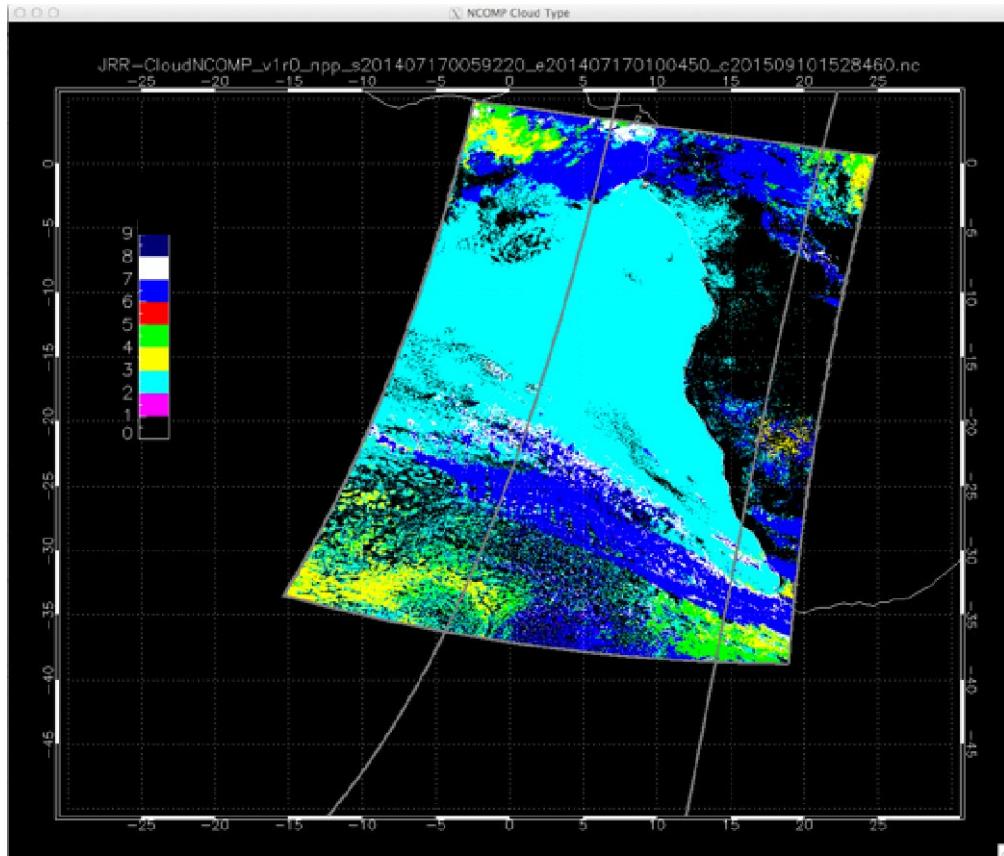
Figure 6. Cloud phase input from VIIRS Cloud Phase/Type algorithm for ~0059 UTC, 17 July 2014. The Cloud Type is collapsed as in Table 4 for usage in NCOMP.

4.2 Output from Simulated Input Data Sets

Preliminary NCOMP products in HDF files were generated using the NPP VIIRS data for several test cases during the 2.5-month validation period. Figures 7-10 show the NCOMP output for cloud optical depth, cloud particle size, liquid water path and ice water path. Figs. 7, 8, and 9 images correspond to 0059 UTC, 17 July 2014 and Fig. 10 corresponds to 0830 UTC, 6 January 2015. The latter was chosen due to the presence of more ice clouds.

The water cloud optical depths (Fig. 7) off the west coast of central and southern Africa are mostly larger than 5, with values decreasing to as low as 1.0 as you approach the edges of the large, solid stratocumulus cloud masses that are typical of this regime in Southern Hemisphere winter months. Over the comparatively broken stratocumulus to the south, cloud optical depth shows more variability, as expected, as does cloud particle size (Fig. 8). The radius retrievals appear to be somewhat homogeneous over the solid stratocumulus deck with most r_e(water) values ranging from 6.0 to 15.0 μm. There is, however, more variability in r_e(water) over the broken stratocumulus to the south with

38

values between 8 and 32 μm, with the larger perhaps indicating some impact from subscale clouds and even contamination from very thin cirrus clouds.
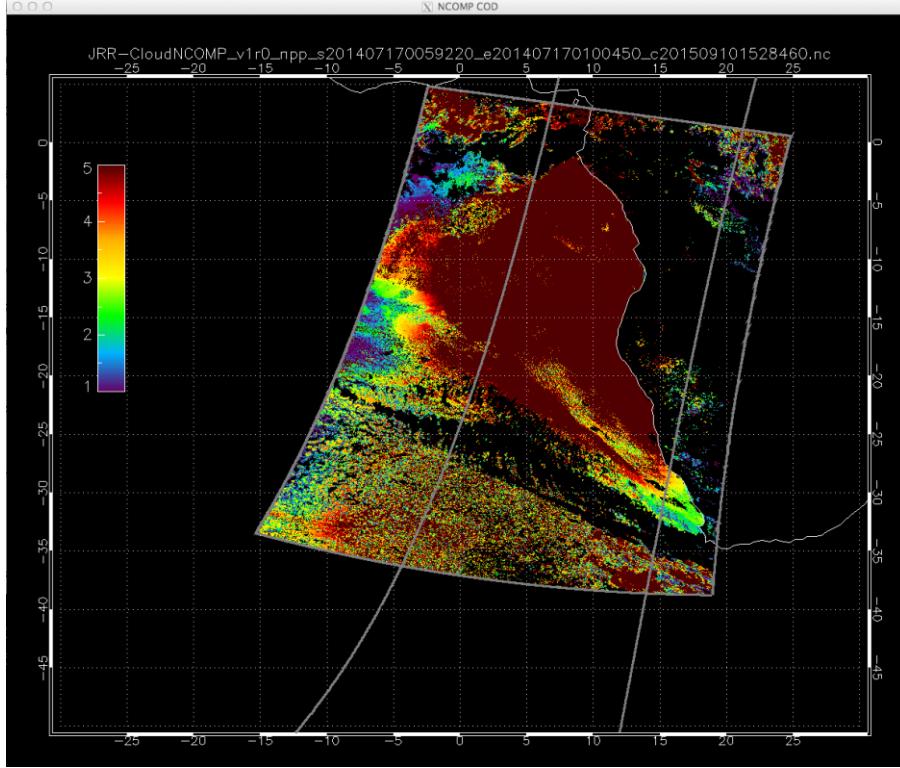
Figure 7. Example of output water cloud optical depth from VIIRS NCOMP algorithm for ~0059 UTC, 17 July 2014.

Since most of the retrieved optical depths and particle size values are very small, the resulting LWP values (Fig. 9) are quite small with most values < 50 gm^{-2}. Larger values are found only where the algorithm returned the maximum optical depth and larger r_e(water). In those instances (red in Fig. 9) LWP > 100 gm^{-2}. The IWP values (Fig. 10) are much more variable, primarily because r_e(ice) for this image is fairly homogeneous. Small changes in τ yield significant changes IWP on the scale shown in Fig. 10.

It is clear from these figures that the NCOMP is producing robust results, but not necessarily at the level expected when compared with SIST. For example, Figure 11 shows the results of applying the SIST, outside of the offline framework, to a Meteosat-9 SEVIRI image (Fig. 11a) taken at 2215 UTC, 17 June 2008. The phase (Fig. 11b) colors are different than those in Fig. 6 with green indicating clear and liquid and ice water shown in blues and red, respectively. The optical depths (Fig. 11c) range from less than 1 for many ice clouds up to 32 for some of the convective clouds. The values of r_e(water)
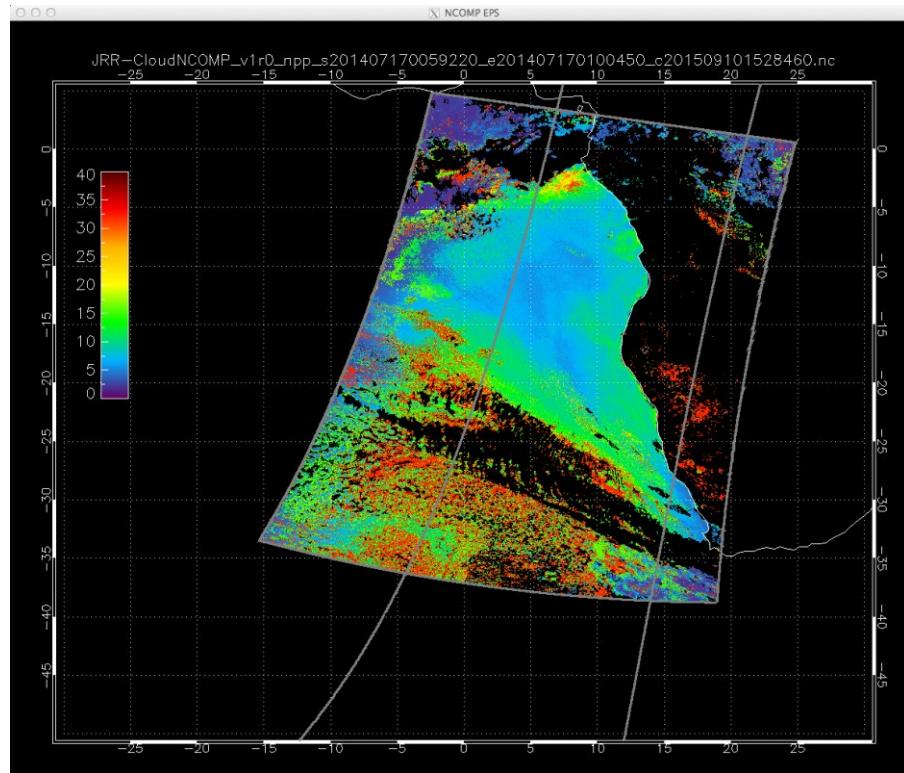
Figure 8. Example of output cloud particle size (μm) from VIIRS NCOMP algorithm for ~0059 UTC, 17 July 2014.
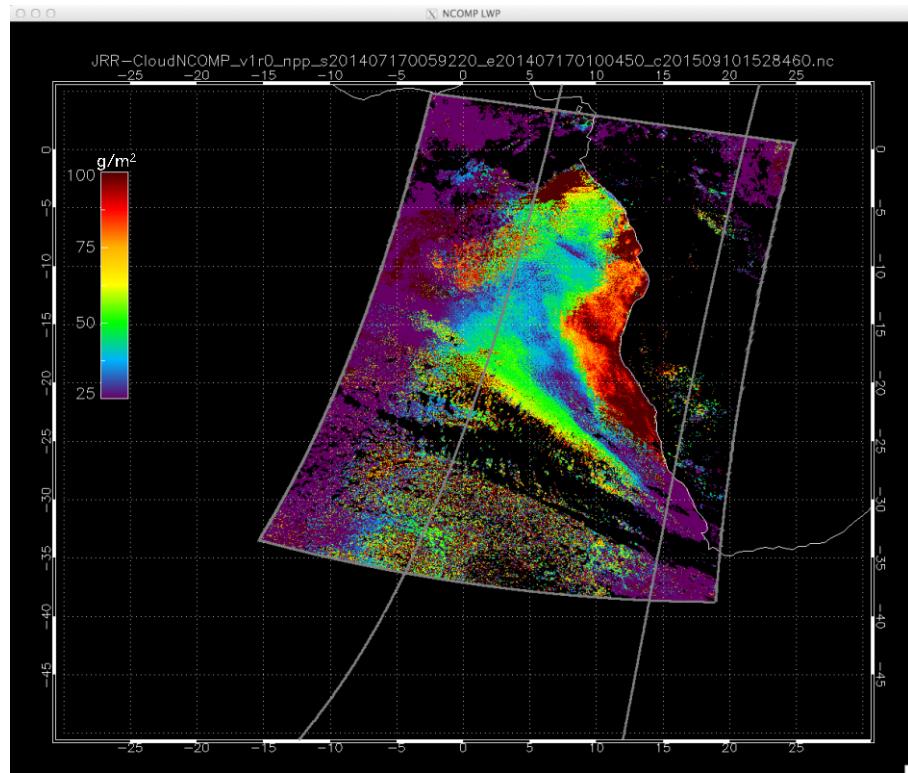
Figure 9. Example of output cloud liquid water path (g m⁻²) from VIIRS NCOMP algorithm for ~0059 UTC, 17 July 2014.
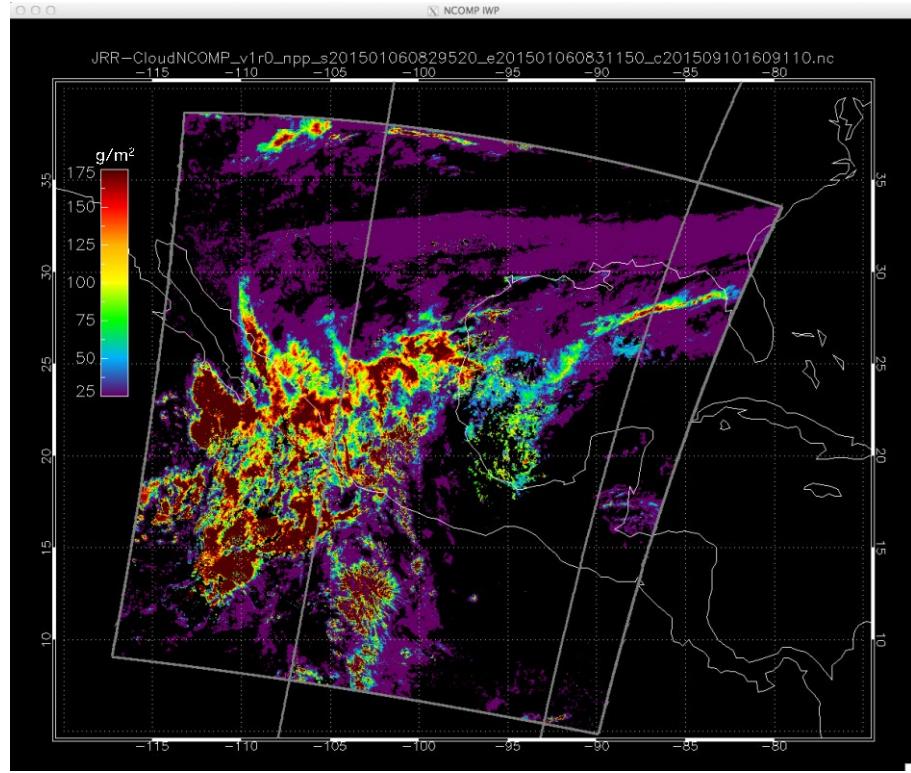
Figure 10. Example of output cloud ice water path (g m^{-2}) from VIIRS NCOMP algorithm for for ~0830 UTC, 6 January 2015.

in Fig. 11d range from 6 µm over Brazil to > 25 µm over some of the ocean areas. Values for D_e (Fig. 11e) vary from < 15 µm up to the maximum value. A smaller percentage of D_e values are at the maximum compared to Fig. 8. The LWP values (Fig. 11f) also show a greater range than seen in Fig. 9, with many values exceeding 50 gm^{-2}. These differences in the character of the results suggest that some input variables used in the NCOMP still need to be examined closely, especially the surface emissivities and radiative transfer calculations. The earlier versions of NCOMP have also been hampered by using the nominal 3.7- or 3.9-µm channel calibration. The impact of this assumption is discussed in 4.2.1.3.
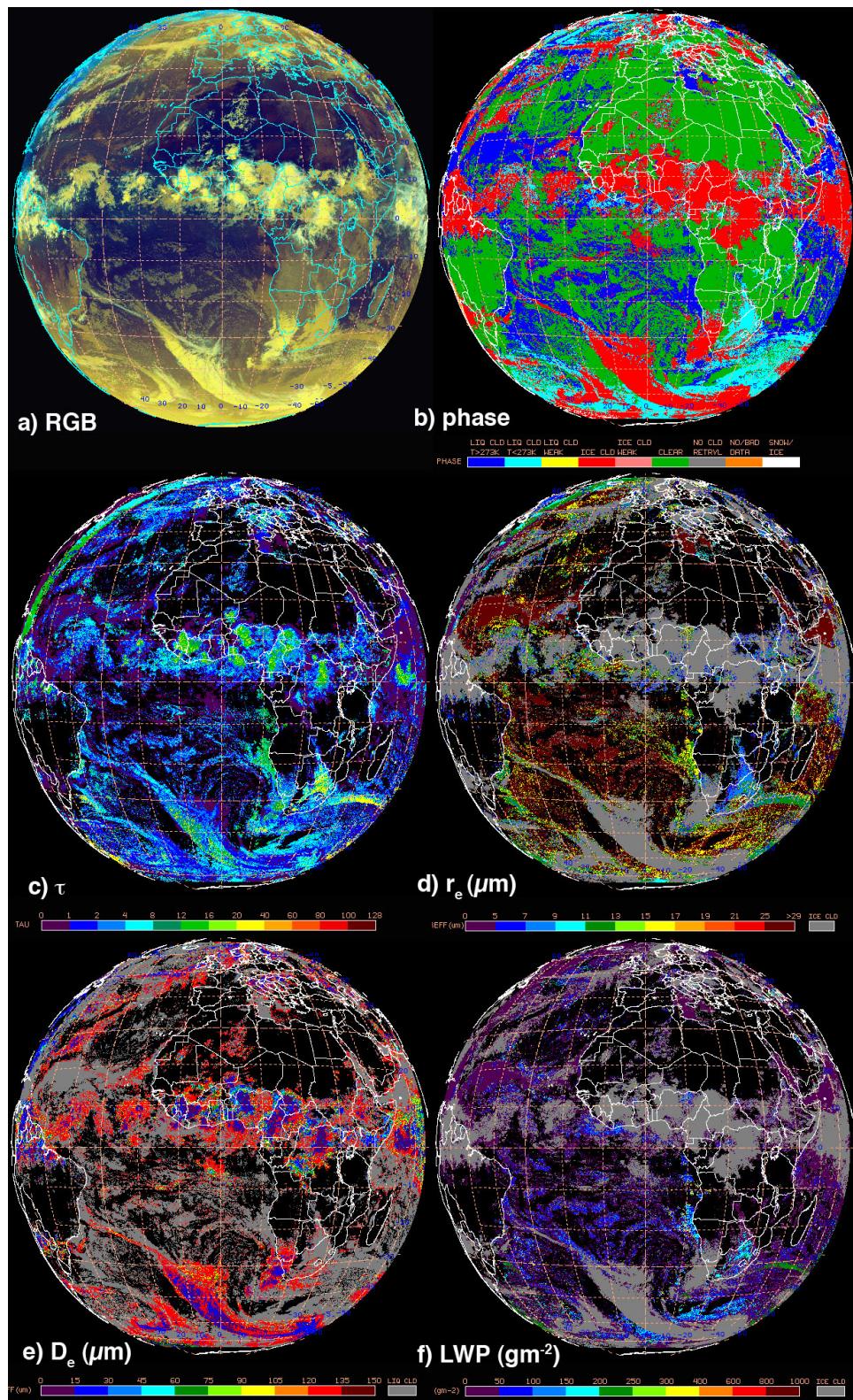
Figure 11. Cloud properties retrieved from Meteosat-9 NPP VIIRS using the SIST, 2215 UTC, 17 June 2008.

4.2.1 Precisions and Accuracy Estimates

The precision and accuracy of the results of the NCOMP can be determined both theoretically through sensitivity studies and via comparison with independent, presumably, more accurate measurements.

A set of sensitivity studies was conducted to fully define the accuracy and precision of each retrieved parameter. The results indicate that both accuracy and precision specifications are being met. These analyses explored the sensitivities of the retrievals to errors in surface emissivity and temperature and T_{cld}, and the cloud-surface temperature contrast for a wide range of conditions and particle sizes. These sensitivity studies, discussed in 4.2.2, enabled the specification of more reliable limits for the algorithm.

Uncertainties in the NCOMP cloud optical depth, particle size, LWP and IWP can be also be estimated by quantitative comparisons with coincident data from several sources:

1. Surface-based remote retrievals

2. Aircraft-based in situ retrievals

3. Satellite-based remote retrievals

As with any property retrieved from satellite instruments, direct comparisons can be difficult due to time and space matching issues, differences in algorithm assumptions and spectral variations. Regardless, extensive validation of NASA Langley's SIST has been performed using the full SIST algorithm. Once any inconsistencies between SIST and NCOMP results from the offline framework have been identified and eliminated, it is anticipated that the NCOMP validation effort will yield similar results as the algorithms' underpinnings are the same.

4.2.1.1 Cloud Optical Depth

Cloud optical depth and r_e can be estimated directly by flying an aircraft through a target cloud making complete vertical profiles of cloud particle sizes and number densities [e.g., Eq. (3)]. Historically, such profiles are few and far between during daytime. Even rarer is the nocturnal profile. Thus, for comparison to NCOMP retrievals, τ and r_e have to be determined indirectly from remote sensing instruments. A variety of techniques (e.g., Liu and Illingsworth, 2000; Dong and Mace, 2003; Mace et al., 2005) have been developed to use uplooking microwave radiometers, lidars, cloud radars, and infrared radiometers to retrieve LWP/IWP and r_e, and, hence, τ. Even multispectral infrared radiometers have been used alone to retrieve τ and r_e for semi-transparent clouds without the aid of other instruments (e.g., Turner and Holz, 2005). Such measurements have been
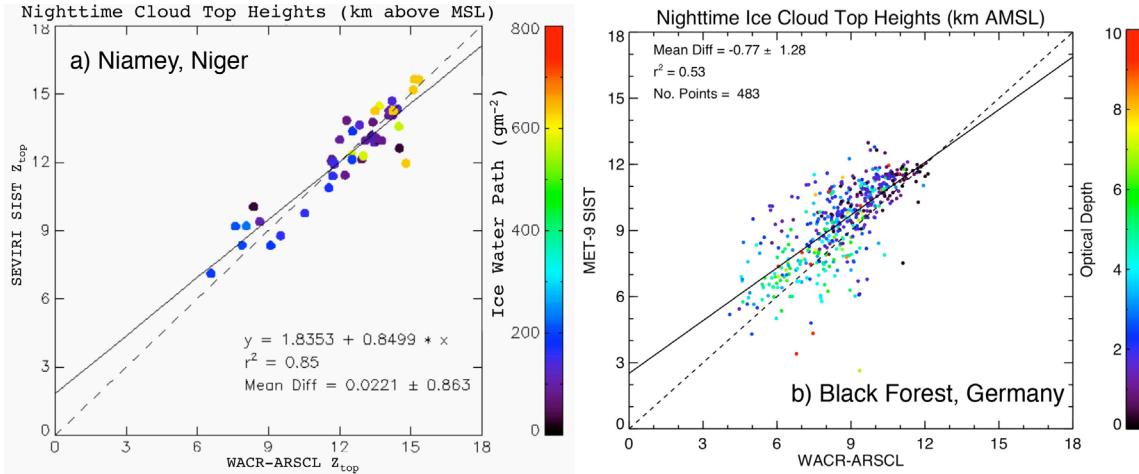
Figure 12. Comparison of SIST cloud top heights (km) from SEVIRI data and surface-measured cloud top heights from the AMF active sensors. (a) April – October 2006, SIST-derived IWP shown in color. (b) April – December 2007, SIST optical depth shown in color.

used extensively for daytime comparisons and should be applied more often to nocturnal retrievals. Lidars at the surface and on aircraft and satellites are all also used to retrieve thin cloud optical depths and particle sizes (e.g., Chiriaco et al., 2004, 2007). The infrared optical depths of optically thin clouds can be inferred from the heights of clouds. Thus, if the derived height is correct after correcting for semi-transparency, then τ must also be correct.

An example of that last approach is seen in Figure 12, which shows comparisons of ice cloud height obtained using SIST applied to SEVIRI imagery and from surface-based remote retrievals using combined radar, lidar and ceilometer products over the Atmospheric Radiation Measurement (ARM) Program Mobile Facility (AMF) when it was deployed at Niamey, Niger from April - October 2006 and over a site in the Black Forest in Germany from April - December 2007. The accuracy of the cloud heights for these ice clouds indicates that cloud optical depths are also quite accurate given that the cloud temperature is directly related to the cloud optical depth and emittance.

A similar comparison of cloud heights was performed over the ARM Southern Great Plains (SGP) by Smith et al. (2008) and showed very good agreement between the radar and SIST cloud top heights from GOES for optically thin clouds, indicating good agreement in cloud optical depth for the thin clouds.

The cloud optical depths can also be compared with MODIS-derived optical depths and particle sizes from the Cloud and Earth's Radiant Energy System (CERES) project, which are derived with SIST. This data set covers the entire globe for many years hence the full disk of SEVIRI results will be able to be compared with the MODIS optical depths. The comparison will provide a multitude of consistency checks as well as a validation of NCOMP's ability to produce similar results for multi-angle views of the same scene. Another consistency check is determine if the optical depths change

drastically between day and night in the absence of a pronounced, rapidly changing convective cycle. For example, Fig. 13 shows an example of the mean τ and r_e for liquid
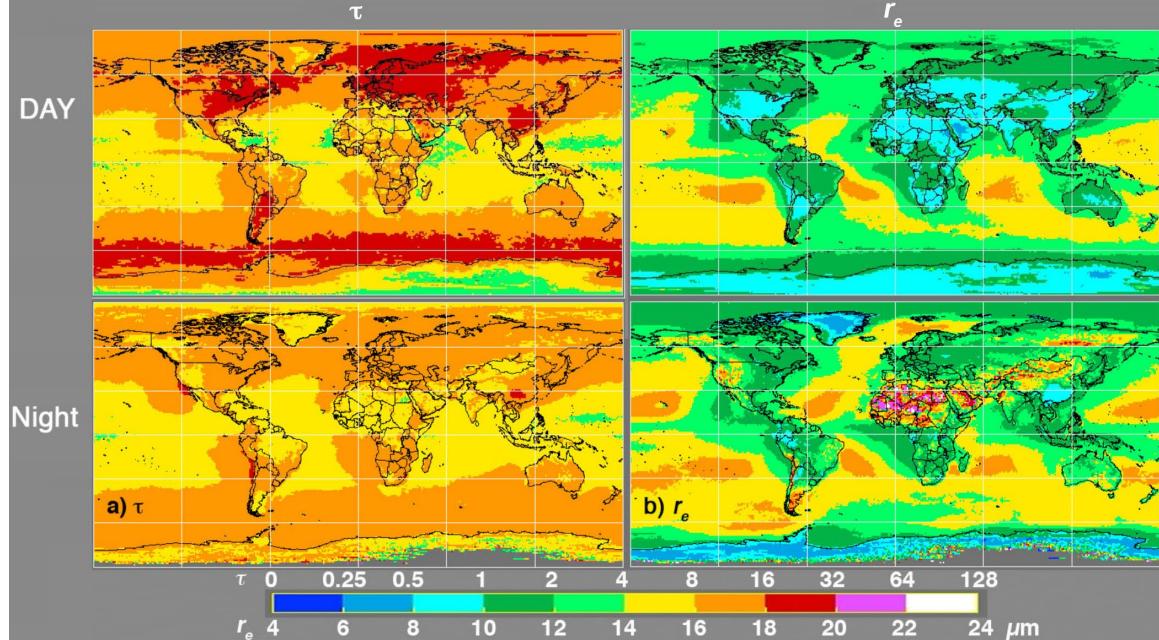
Figure 13. Mean liquid water optical depths and effective droplet radii derived from Terra MODIS data for CERES using the VISST (day) and SIST (night), 2001-2006.

water clouds derived from Terra MODIS data using the VISST during daytime (top row) and SIST at night (bottom row). Keeping the optical depth and particle size limitations of the SIST, the patterns in the mean values of both parameters are quite consistent over ocean. Over land areas, there is less consistency owing to the variability in ε_s and uncertainties in T_s, especially over deserts.

4.2.1.2   Cloud Particle Size

Figure 14 shows a case study comparison of ice cloud τ and r_e obtained using SIST applied to GOES imagery and analogous quantities derived from surface-based remote measurements using a surface-based interferometer (AERI) and Raman lidar (CARL) over the ARM Southern Great Plains (SGP) site for 2 nights, 8 November 2000 (Fig. 14a) and 29 November 2002 (Fig. 14b). The cloud boundaries from the lidar are also shown. The optical depths from satellite, indicated by the red diamonds, compare very well with the surface-based optical depths from AERI and CARL.

The AERI-derived particle sizes, while exhibiting a great deal of variation over this time scale, also compare fairly well with the SIST-derived r_e, although the absolute accuracy is difficult to assess given the high temporal resolution of the AERI and the low temporal resolution of GOES.

An example of comparisons with liquid water clouds is shown in Fig. 15 for data taken over the ARM SGP site for cases of overcast stratus clouds corresponding to Aqua MODIS overpasses. The SIST retrievals are shown as the solid symbols. The open symbols represent the retrievals from the surface using the method of Dong and Mace
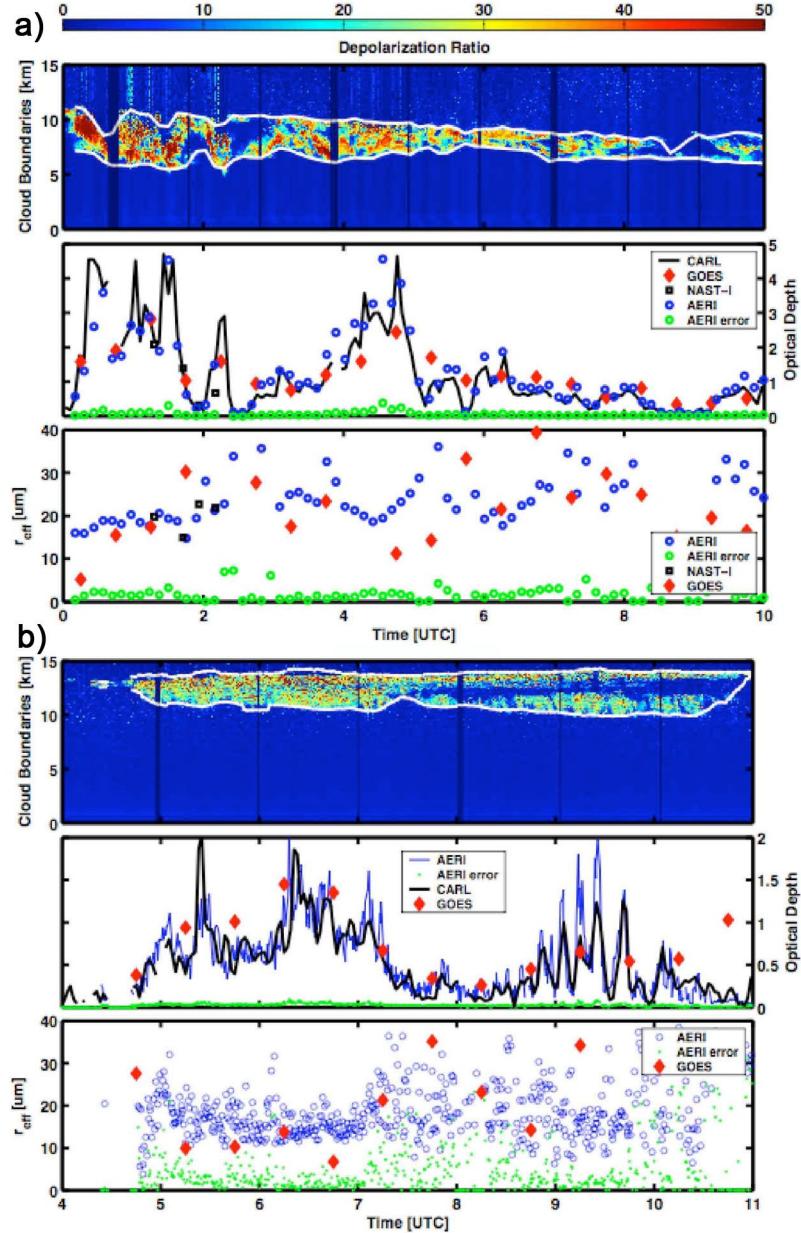
Figure 14. Comparison of SIST cloud optical depths and cloud particle sizes from GOES data and surface-measured quantities from surface interferometer (AERI) and Raman lidar (CARL) at the ARM SGP. (a) 8 November 2000. (b) 29 November 2002. CARL depolarization and cloud boundaries are shown in the top panels (personal communication, D. Deslover).

(2003) applied to the ARM radar and microwave radiometer data. On average, there is excellent agreement between results, but the correlation is relatively low. The highest squared correlation coefficient, found for τ, is 0.4. Greater correlation is found for all parameters, if only thinner clouds are compared. Similar datasets have been taken by the AMF over Germany and can be used in the same type of analysis to help validate the SEVIRI retrievals.
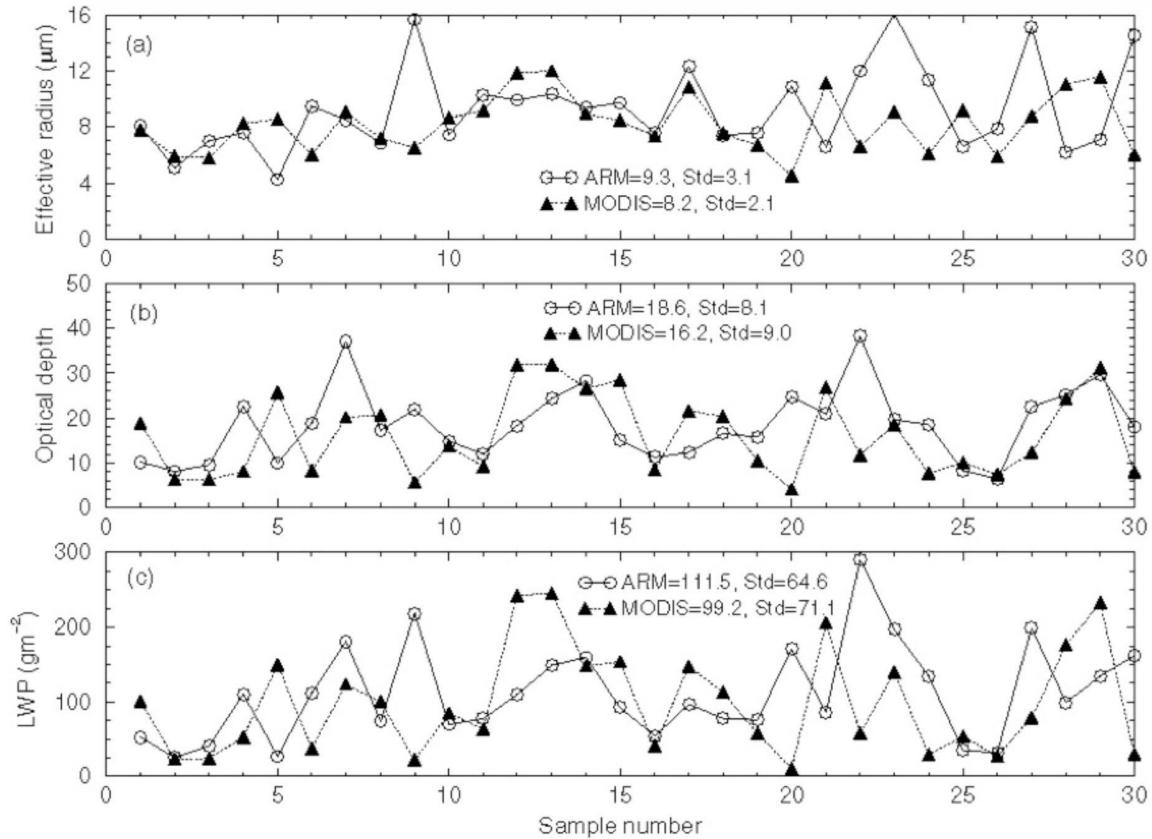
Figure 15. Comparison of mean cloud properties over the ARM SGP using surface-based measurements (ARM) and the SIST (MODIS) applied to nocturnal Aqua MODIS data, 2002-2005, for single-layer overcast stratus clouds. Each point represents a 15-min average from the surface data and a 30 km x 30 km average of satellite pixels. (personal communication, X. Dong).

4.2.1.3 LWP and IWP

The LWP and IWP retrieved from SIST have been compared with surface and airborne data as described above. As with the other NCOMP output, the liquid water path and ice water path can also be compared with MODIS-derived LWP and IWP from the CERES project, also derived with SIST or from NPP VIIRS using SIST. An added benefit of comparing NCOMP and SIST results to each other is that consistency checks can reveal any retrieval artifacts due to instrument calibration issues. A comparison of NCOMP and SIST IWP derived from the same SEVIRI images over Europe over 3-4 August 2006 is shown in Figure 16. An easily identifiable feature in comparing these results of IWP to

each other is an apparent bias, particularly at the higher values of IWP for thicker VIIRS Cloud Types of Ice and Overlap. As there is no spatial or temporal discontinuity to contend with, a fair conclusion might be that NCOMP has a high bias with respect to the better-validated SIST IWP retrievals.
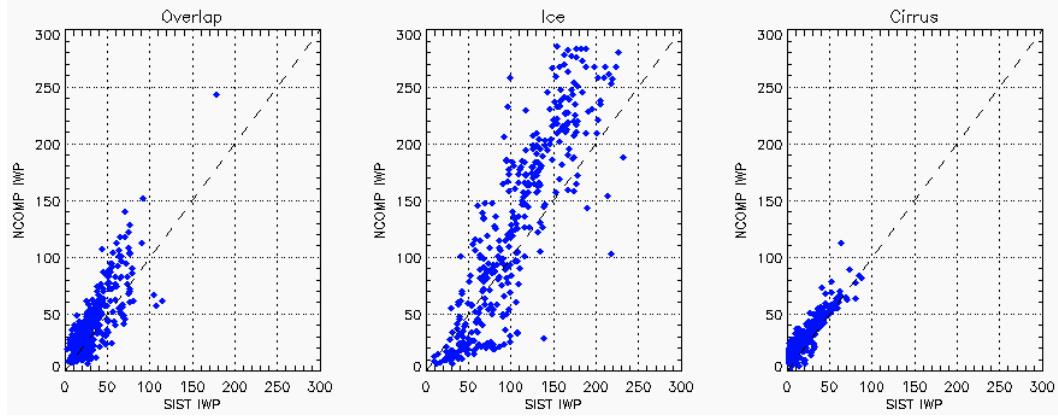
Figure 16. Comparison of NCOMP and SIST IWP for 3-4 August 2006 over Europe, separated by ABI Cloud-Type.

The bias, however, appears to be primarily the result of calibration differences. The SIST retrievals were performed in NASA Langley's framework utilizing recalibrated data while the NCOMP retrievals were conducted in the GOES-R developmental framework using the nominal SEVIRI calibrations for each channel. The NASA processing uses a robust calibration correction (Minnis et al., 2006) to the 3.7-μm channel that is based on comparisons between GOES-12 and SEVIRI with an example shown in Figure 17. The slope of the intercalibration appears to be almost identical to that of the IWP
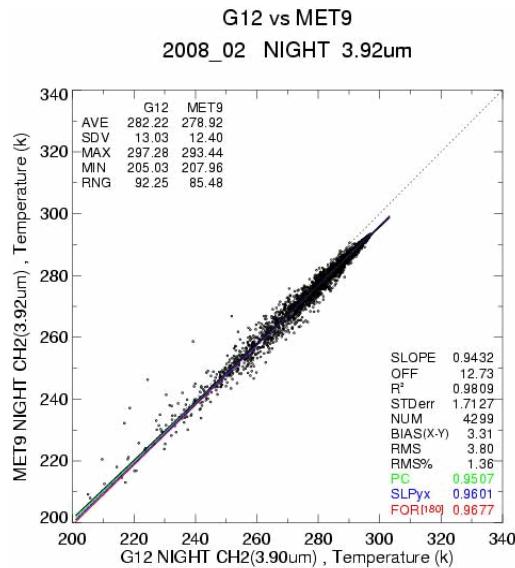
Figure 17. Calibration between spatially and temporally matched nighttime GOES-12 (G12) 3.9-μm temperatures and SEVIRI (MET9) 3.9-μm temperatures from NASA Langley.

comparison in Fig. 16, indicating that calibration discrepancies are contributing to an overestimation of NCOMP IWP. Given that 3.9-μm temperature differences as large as 4 K are expected, the bias in IWP has been reduced significantly by implementation in the GOES-R developmental framework for NCOMP (not shown). Due to the impact of calibration differences, the ability to modify radiances has been integrated into the NCOMP (see description of the Calibration Coefficients in 3.3.2). Currently, the coefficients are simple linear corrections, i.e., a slope and an offset, that are given for and applied only to the Channel 3.9μm temperatures. Should other channels, including the 10.8-μm channel, need to be recalibrated in the future, new coefficients will be provided and the data files will be enlarged to include those coefficients.

Other efforts for validation of LWP and IWP are discussed in 5.5.3.

4.2.2 Error Budget

The error budget relies both on the retrieval validation and on the accuracies of several of the input parameters, as well as the parameterization uncertainties. The accuracy and precision estimates were developed based on detailed sensitivity studies and available empirical comparisons are analyzed in detail, but current results are presented in Table 8. The accuracies and precision estimates are extracted from the discussion of 5.5. While some of the requirements for which no direct comparison is indicated, we anticipate being able to complete them using limited case study-derived data because more thorough data sets are not available. The sensitivity analyses are presented below.

Table 8. Current NCOMP Accuracy and Precision Estimates Compared to F&PS Requirements. Red values indicate current NCOMP performance while * indicates a preliminary result that is further discussed in 5.5.

| Product	Measurement Range	Measurement Accuracy	Measurement Precision
COD	1.0 – 5.0 1.0 – 5.0	30% 7.3%	max of 0.8 or 30% 0.63%
CPS	liquid: 2 < CPS < 32μm 2 < CPS < 32μm ice: 2 < CPS < 50μm 2 < CPS < 50μm	liquid: max of 4μm or 30% *no direct comparison ice: 10μm *no direct comparison	liquid: max of 4μm or 25% *no direct comparison ice: max of 10μm or 25% *no direct comparison
LWP	25 < LWP < 100 gm^{-2} 25 < LWP < 100 gm^{-2}	greater of 25 gm^{-2} or 15% 6.05 gm^{-2}	greater of 25 gm^{-2} or 40% 22.09 gm^{-2}
IWP	25 < IWP < 175 gm^{-2} 25 < IWP < 175 gm^{-2}	greater of 25 gm^{-2} or 30% *no direct comparison	greater of 25 gm^{-2} or 40% *no direct comparison

A detailed sensitivity analysis was performed for the NCOMP algorithm using the uncertainties expected in the input variables from upstream in the process. A Jacobian analysis was used wherein the brightness temperature for each channel was first calculated for the unperturbed case and then recalculated using the perturbation corresponding to the input parameter uncertainties. In some cases a larger value was used and interpolation was employed to arrive at the true uncertainty value. Uncertainties in the surface emissivity ($\pm$ 0.02), surface skin temperature ($\pm$ 2.5 K), relative humidity ($\pm$15%), and T_{cld} ($\pm$ 2 K for water, $\pm$ 3.5 K for ice) were considered. Calibration errors are considered small by comparison and were not evaluated. The calculations were performed using local zenith angles between 25 and 55° using standard atmospheric profiles and a range of COD and CPS for both ice and water clouds.

Each error was considered individually and in combination as random errors to obtain the RMS uncertainty resulting from errors in the input values. The sensitivity analysis is summarized in Fig. 18 for water and ice clouds separately. The COD errors vary between 22 and 28% for water clouds (Fig. 18a) and 15 and 32% for ice clouds (Fig. 18b). The
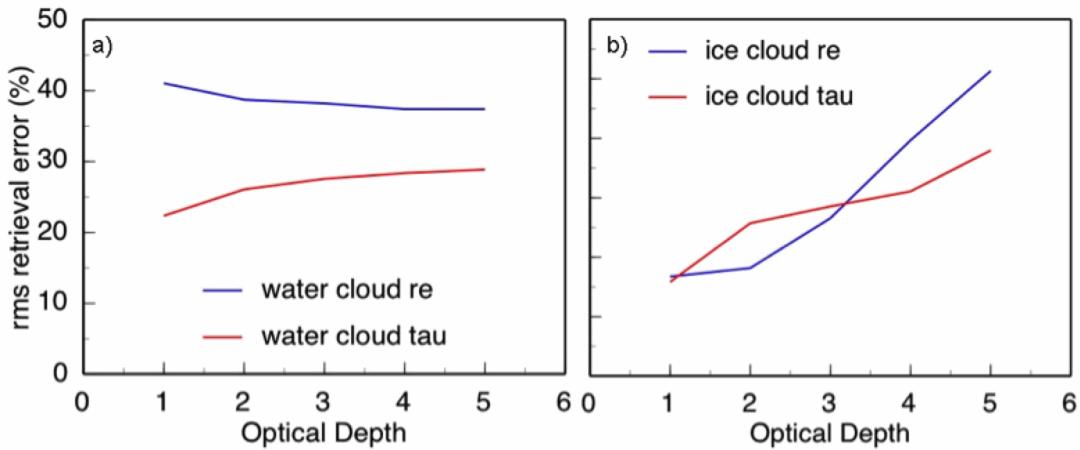
Figure 18. Summary of sensitivity errors of NCOMP COD and CPS (re), shown as RMS error of all input uncertainties combined. Larger errors were obtained for COD outside the range of 1 – 5.

errors increase rapidly for COD > 5 and COD < 1, particularly for ice clouds. The retrieved CPS errors are somewhat larger, around 40% for water and between 15 and 42% for ice CPS. The average ice cloud CPS RMS error is ~25%. These uncertainties meet both the current and pending F&PS requirements in most cases. The only exception is the water CPS.

5 PRACTICAL CONSIDERATIONS

5.1 Numerical Computation Considerations

The NCOMP is implemented sequentially. Because the algorithm relies on the values of the ancillary data, the radiative transfer model, NWP data set and the performance of the Cloud Height/Temperature and Cloud Phase/Type algorithms, these quantities need to be computed first.

5.2 Programming and Procedural Considerations

NCOMP is purely a pixel by pixel algorithm and requires no knowledge of the VIIRS or ABI radiances or cloud properties of the adjacent pixels. Results will not vary if larger or smaller amounts of imagery are processed. Several iterative steps are involved in NCOMP, but these are well tested in an operational setting. No forward calculations or look-up tables are required other than the calibration and emittance parameterization coefficients.

5.3 Quality Assessment and Diagnostics

The quality assessment information in the form of the quality and processing flags of Table 6 and Table 7, which are listed in sections 3.4.3.2 and 3.4.3.3, respectively, are used to monitor the performance of the NCOMP. A Quality Flag of 0 indicates that the retrieval was performed successfully while a non-zero value indicates that the retrieval was not performed with the reason given by the values detailed in Table 7. The Processing flags are used for all pixels for which successful retrieval was performed. A non-zero Processing Flag bit reflects the path taken in the algorithm or what may be a physically important consideration, as in Table 6. Multiple Processing bits can be turned on because the algorithm paths are not independent.

In Table 7, the Quality Flag values are self-explanatory with the exception of the values of 6 or 7. These values are not likely to occur, but if there were to be a problem reading in the emittance parameterization coefficients described in 3.3.2 indicate that there is likely a problem either with the ingestion of the coefficients or with the coefficients themselves.

The Processing Flag values in Table 6 provide valuable validation information as well as tools for the user who may need to know how a particular solution was chosen. For example, if Processing Flag bit 1 is turn on, then the pixel is from twilight when NCOMP provides only qualitative results that are not expected to meet the F&PS requirements. In these situations the cloud properties are indeed present, but users will need to understand that they are potentially of a degraded quality. Other Processing Flag bits provide the

potential for feedbacks between NCOMP's minimum error solution, described in 3.4.2.2, and the Enterprise Cloud Type. If the minimum error solution appears to be for a different Cloud Type than indicated by the input Cloud Type, for example, then the appropriate bit, 2 through 7, would be turned on. NCOMP, however, is currently not retrieving both water and ice solutions for a particular pixel due to latency concerns; hence these 6 bits are reserved for future and/or diagnostic implementation. Similarly, if the potential for phase ambiguity is thought to be high, e.g., for overlap clouds, a Processing Flag bit will indicate this using the appropriate bit, 8 or 9. When either of bits 10 through 13 is on, it is an indication that the chosen CPS solution was exactly the smallest or largest model, i.e., the actual value very likely falls outside of the range of the CPS models. Note that the Processing Flags have no impact on the NCOMP cloud products; they detail the chosen solution's path in the algorithm and/or indicate that NCOMP is not necessarily yielding the best results for the situation described by the inputs or that the clouds are of a particular difficult variety.

5.4 Exception Handling

The NCOMP includes checking the validity of the derived VIIRS or ABI inputs before applying the algorithm. The NCOMP expects the main processing system to flag any pixels with missing geo-location or solar and viewing geometry information.

The NCOMP does not check for conditions where the NCOMP cannot be performed or will return unreliable results, including saturated channels, missing RTM values or inconsistencies in the TRM data. In these cases, it is assumed that the framework will accomplish these tasks, particularly since NCOMP is late in the processing chain that many other algorithms will have already flagged such conditions, including those that provide derived VIIRS/ABI input to NCOMP. If explicit checking of every possible input is needed, this can easily be addressed.

The NCOMP returns no cloud properties if any of the required inputs, including channel data, are missing.

5.5 Algorithm Validation

In addition to the studies already mentioned, several additional comparisons have been performed to validate the results. Some comparisons use consistency, while others are direct quantitative comparisons. The types of comparisons reviewed in section 4.2.1 will continue to be repeated using offline framework-based NCOMP retrievals based on NPP VIIRS data

5.5.1   Cloud Optical Depth

Aligned with Aqua and CloudSat in the A-Train, the Cloud-Aerosol Lidar and Infrared Pathfinder Satellite Observation (CALIPSO) lidar is used to retrieve τ for clouds having τ < 3. Comparisons with NPP VIIRS will be performed for every overpass for selected periods to assess the uncertainties in τ retrieved by the NCOMP. If CALIPSO or a similar instrument is in orbit after JPSS is launched, its data will also be used to validate τ from the VIIRS. Additionally, it would be possible to simulate the VIIRS algorithm output by defining the cloud heights and temperatures using the CALIPSO and NWP temperature profiles and perform NCOMP on MODIS data matched to Aqua. The results could be compared to similar output from the method of Chiriaco et al. (2004) now being applied to CALIPSO lidar and infrared radiometer data.

A comparison of temporally and spatially matched NCOMP and CALIPSO optical depths from a seasonally and geographically diverse subset of more than 900 nighttime SNPP VIIRS granules taken during a 2.5-month validation period is shown in Figure 19. The CALIPSO measurements are within ± 15 minutes of SEVIRI scan times and the VIIRS pixels closest to each CALIPSO latitude and longitude, yet within 5 km, is chosen for the comparison. The range of τ shown in Fig. 19a is expanded beyond the F&PS requirement to $0 < \tau \leq 6$ to show the robustness of the retrieval beyond its expected performance range and to increase the number of samples, hence bolster confidence in the statistics. In Fig. 19b, the retrievals are limited to exactly the F&PS requirement of $1 \leq \tau \leq 5$ so that any statistics will be directly comparable to the F&PS requirements. While this τ limitation eliminates the majority of cloudy pixels from the comparisons, it is necessary despite the relative paucity of nadir matches for thin clouds and due to the physical limitations of the current version of NCOMP which is reflected in the proposed requirements mentioned in 2.1.

The points in Fig. 19 correspond to VIIRS pixels with VIIRS Cloud Types of ice, cirrus, overlap, and overshooting top, thought to be the most applicable to NCOMP's F&PS requirements, i.e., unambiguous phase. While some of these types are potentially optically thicker and others multi-layer, these types are included to examine NCOMP's performance outside the F&PS range. The expanded COD points (Fig. 19a) have a bias (accuracy) of -0.14 while those in in the F&PS range (Fig. 19b) have a bias of -0.12, corresponding to 13.7 and 7.3%, respectively, verifying that the subsetted Cloud Types show good agreement between NCOMP and CALIPSO. The precisions of both data sets easily meet the F&PS precision requirements.
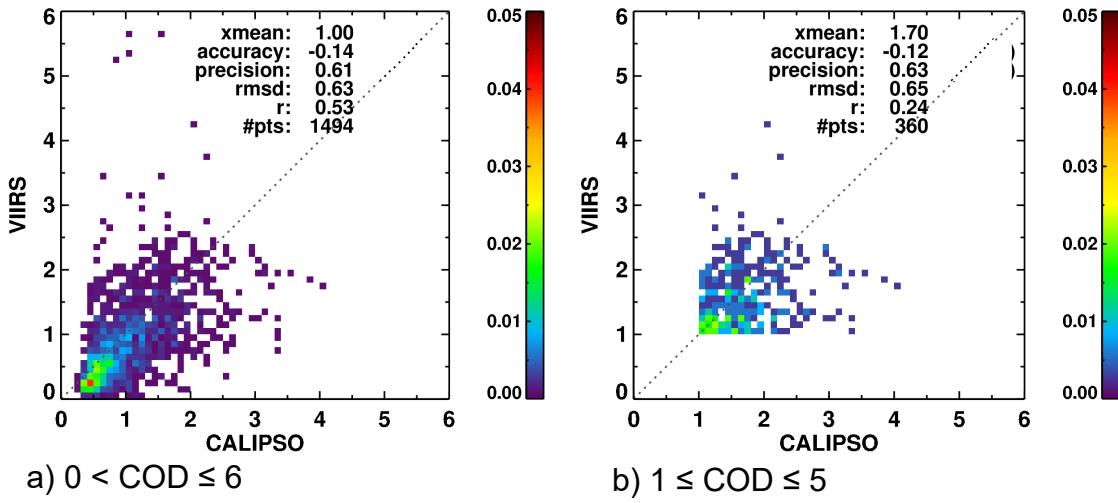
Figure 19. Comparison of matched NCOMP and CALIPSO COD from VIIRS for 900+ granules in the 2.5-month validation period.

The percentage difference of COD, CALIPSO – NCOMP, for a different NCOMP validation set is shown in Fig. 20 as a function of CALIPSO COD. NCOMP for this comparison was applied to SEVIRI data but results from application to VIIRS and ABI are similar. The data are from a seasonally representative 10-week validation period from 2007. It is apparent that the cirrus points, despite generally having the lowest CODs, also have the best agreement with CALIPSO. The overlap clouds also have relatively low differences, despite the fact that the Cloud Type algorithm indicates that they are thin ice clouds over lower water clouds, a situation in which one might conclude that NCOMP would not perform well given its single-cloud layer assumption. The CALIPSO retrieval, however, generally does not include much of the impact of that lower layer as CALIPSO-derived water cloud information is not reliable, so in effect the overlapped pixels are somewhat similar to the cirrus points but with larger τ. Similarly, Cloud Types that are indicative of a water phase, fog, water, supercooled and mixed are also excluded from the eventual statistical comparisons. When Cloud Type = Ice in Fig. 20 the differences are also larger than for optically thin ice clouds (Cloud Type = Cirrus) because these pixels are assumed to be optically thick. While many of these points (dark blue) have CALIPSO COD well under 5, the reliability of those retrievals is questionable due to ongoing calibration and reprocessing issues associated with CALIPSO retrievals and algorithmic shortcomings, so these are also eliminated from that statistics. As indicated by one of the CALIPSO Program scientists, liquid water cloud optical depths are not reliable (C. Trepte, personal communication, 2009). Thus, the only statistics that have merit for this comparison are those for semitransparent ice clouds. Those statistics are reported in Table 8.
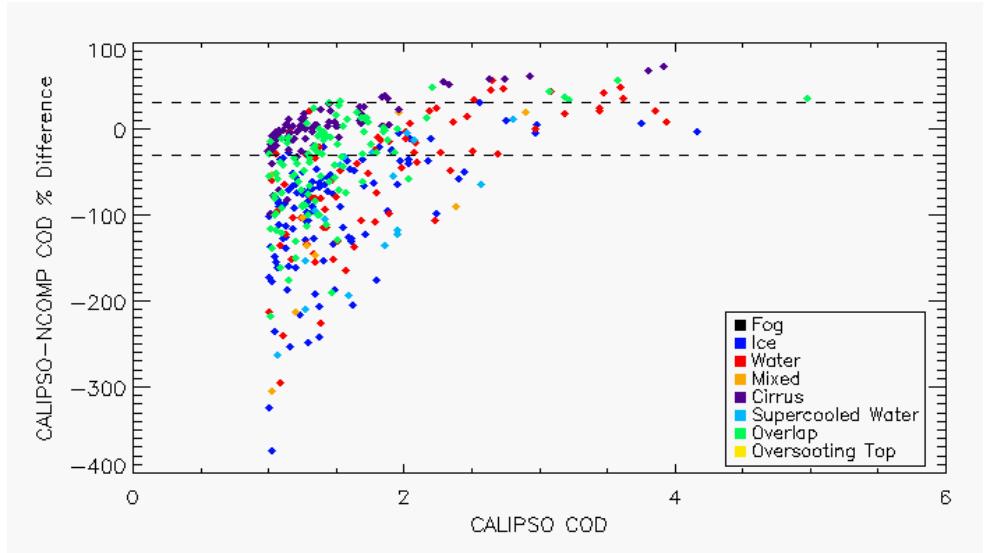
*Figure 20. Percentage differences between NCOMP and CALIPSO COD for data in Fig. 18 with ABI Cloud Type indicated by color.*

Using only the most reliable CALIPSO COD points in Fig. 20, those associated with ABI Cloud Type of Cirrus the bias has improved from -0.451 to +0.084 (or 1.32%), well under the required bias of 30%. For this same set of cirrus-only points, the accuracy is 0.49 or 30.0%, also within the required accuracy, the maximum of 0.8 or 30%.

For single-layer water clouds with $1 \leq COD \leq 5$, ongoing comparisons with CloudSat-derived COD continue to be an option for validation, but first comparisons have not yielded sufficient results. This is expected for several reasons, but the largest hindrance is CloudSat's usage of Radar-Only (RO) retrieval techniques at night. During daylight hours when MODIS algorithms do retrieve COD, CloudSat uses MODIS COD to constrain and bolster the RO retrieval, providing superior results, but at night there are no MODIS retrievals of COD, so CloudSat products are still considered experimental and evolving due to the limitations of the RO technique. Additional source of error are CloudSat's inability to detect some optically thin clouds and water clouds with bases below 1 km, as all as NCOMP's relatively small range of retrievable CODs.

Data from well-equipped surface observatories in Europe (Illingworth et al., 2007) as well as the AMF campaign datasets (e.g., Niamey and Black Forest) discussed earlier will continue to be used to validate JPSS NCOMP optical depth retrievals using the various methods mentioned in section 4.2.1. Validation using surface data will be extended to other time periods to take advantage of these sparse, but relatively well-tested validation sources for COD, as well as LWP, and potentially CPS and IWP. Post-launch data from the ARM sites will also be used for comparison with the VIIRS and ABI retrievals.

A less quantitative, yet useful method for validating the results is by comparing the nighttime retrievals to the nearest daytime retrievals over the same area. Figure 21 shows an example of the daytime VISST and nighttime SIST applied to SEVIRI data at 1500 and 1800 UTC, 6 August 2009. SIST results were used rather than NCOMP because the

56

NCOMP twilight retrievals are required only to be qualitative, hence not as robust as the more reliable twilight SIST retrievals, and because direct comparison was easier due to VISST being run only in a NASA Langley framework. The RGB images (Figs. 21a and b) show the terminator and the cloud structure quite distinctly. Off the east coast of southern Africa, the structure of the low-cloud optical depths is maintained relatively intact although τ has decreased overall. The high clouds to the south, which had relatively large values of τ at 15 UTC, have maximum values of only $\tau = 4$ at 18 UTC. This drop in the high cloud optical depths is likely due to much of the high cloud cover being relatively thin and over optically thick low clouds. Thus, during the daytime, the total optical depth is retrieved, while, at night, only the high cloud optical depth is retrieved because the value of T_{cld} from using the 13.3-µm channel (similar to the Enterprise algorithm) was used in these SIST retrievals. The identification of most of these clouds as multi-layered (Fig. 22) using the algorithm of Chang et al. (2009) confirms the result. In other areas (e.g. central Africa) where high clouds were optically thick from deep convective activity, the patterns in τ follow the thick clouds seen in the RGB image (Fig. 21b) and in the 15-UTC τ image (Fig. 21c).
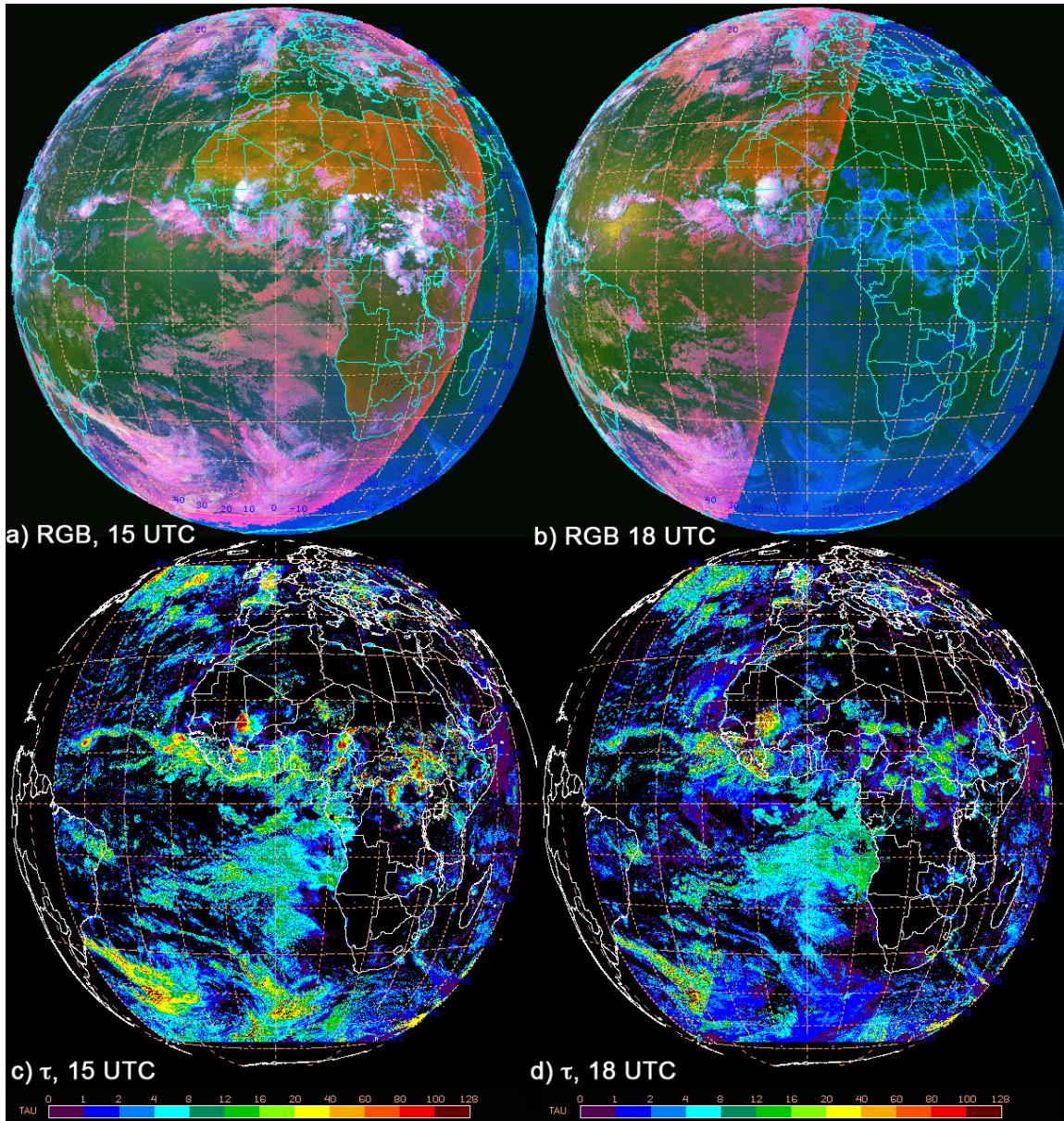
Figure 21. Meteosat-9 SEVIRI imagery (RGB) and retrieved cloud optical depths (τ), 6 August 2009.

The examples in Figs. 21 and 22 show how sequences of data can be used to quickly evaluate the results to determine where and in what conditions the algorithm fails or gives unexpected results. Use of hourly or more frequent sequential images and output parameters will be valuable for rapid visual assessment of the NCOMP output so that potential problem areas can be identified and selected for further study.
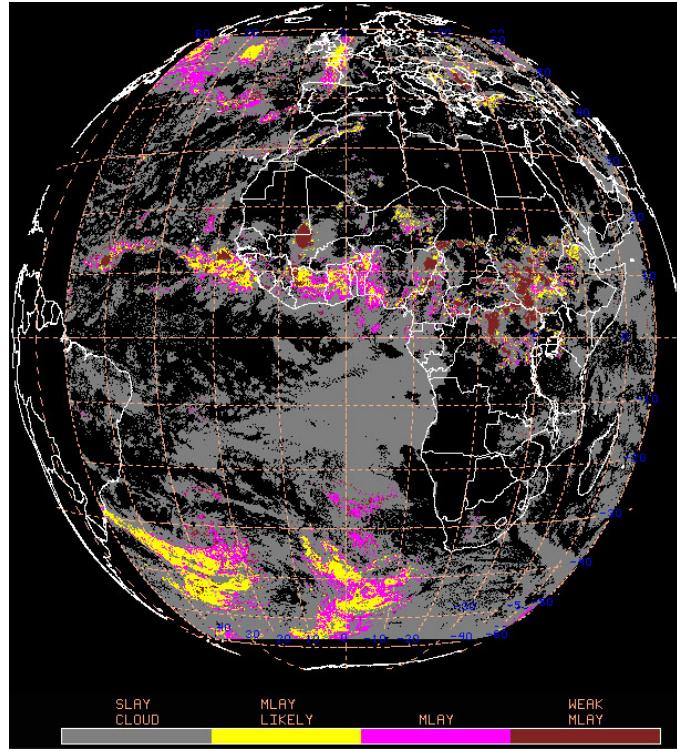
Figure 22. Multi-layered cloud probability, SEVIRI, 15 UTC, 6 August 2009. Gray denotes single-layered clouds, yellow: likely multi-layered clouds, magenta: definite multilayered clouds, brown: possible multilayered clouds, but more likely, a very thick contiguous water-ice cloud system.

5.5.2   Cloud Particle Size

The validation of cloud particle size will follow the same path used to evaluate the optical depth. In most cases, the assessments will be performed on both parameters using the same datasets. The results below discuss comparisons of SEVIRI CPS retrievals, bu the strategy and results are similar for JPSS VIIRS and GOES-R ABI. Figure 23 shows the retrievals of ice (IWC) and liquid water content (LWC) and r_e profiles from radar and microwave radiometer retrievals over two
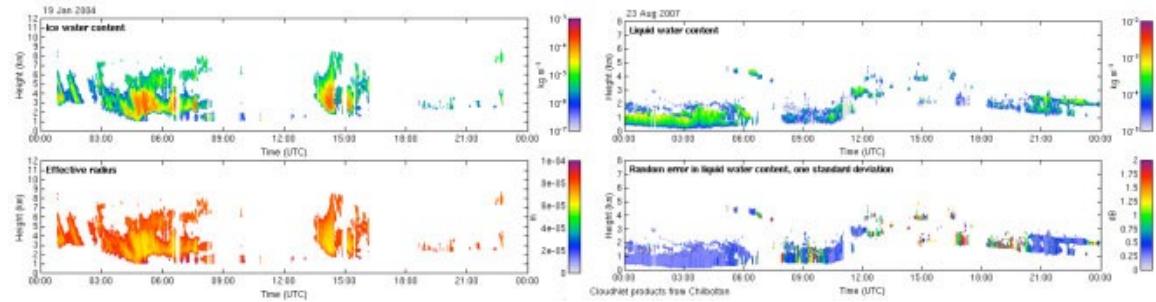
Figure 23. Retrievals of ice water content (top left) and r_e (bottom left) at Palaiseau, France, 19 Jan. 2004 and liquid water content (top right) and error (bottom right) at Chilbolton, UK, 23 Aug 2007.

CLOUDNET sites, SIRTA in Palaiseau, France (left panels) and Chilbolton, UK (right panels). The LWC and IWC profiles can be integrated over the cloud thickness to obtain LWP and IWP, respectively. In like manner, the column integrated r_e can be computed for comparison with the SEVIRI retrievals. This same approach can be used with ARM site data and the CloudSat GEOPROF products to provide more spatial sampling. Consistency checks will also be performed as discussed in the previous section.

Due to the surface sites containing only a single SEVIRI pixel, SEVIRI imagery from a large number of months and likely a large number of years will need to be processed with GOES-R cloud algorithms to provide statistically significant amounts of comparisons. Additionally, NCOMP's need to limit comparisons to only single-layer optically thin cases for either water are ice further reduces surface-based validation opportunities.

CloudSat CPS for GOES-R Cloud Types cirrus and water have been compared to CloudSat data during a 10-week validation period, using a method similar to the COD comparisons of 5.5.1. As with COD, the RO CloudSat technique and the still evolving CloudSat algorithms were expected to negatively influence the comparisons. For cirrus clouds with COD between 1 and 5, accuracy specifications were met (-0.2 μm) with the F&PS accuracy being 10 μm, but precision was only 43.9% with a requirement of 25%. Zhang and Mace (2006) found that RO retrievals of CPS have theoretical uncertainty ranging from 50 to 90%, so even this modest agreement is surprising. Generally though, this result indicates that nighttime CloudSat results are not likely to be a robust validation source.

5.5.3   LWP and IWP

Validation of IWP and LWP will also follow the same approaches used for r_e and τ since the parameters are all linked together. Thus, surface site and CloudSat profiles will be used for validating both IWP and LWP, while the CALIPSO IWC profiles for thin cirrus clouds can also be used for IWP evaluations. One additional dataset will be used to further validate the LWP over ocean, the LWP values retrieved from satellite-borne microwave radiometers. LWP is standard product from the AMSR-2 on GCOM-W. LWP products can be easily matched with the results from the offline framework and compared with either VIIRS and ABI retrievals.

A comparison of NCOMP LWP from VIIRS and AMSR-2 LWP has been done for another subset of the 2.5 month validation period and is shown in Figure 24. Similar to the data shown in Figs. 19 and 20, this comparison was limited to those nighttime points with $1 \leq \tau \leq 5$. A nadir-only comparison is shown (Fig. 24a) along with a full swath comparison (Fig. 24b) when both the VIIRS and AMSR-2 results were averaged onto 0.º5 x 0.5º latitude-longitude grid. The former provides a high spatial resolution comparison opportunity, but limits the number of available matches, while the latter

increases the number of coincident points while degrading the spatial resolution. Additionally, given that many VIIRS pixels were averaged together to mimic the AMSR-2 footprint size or a latitude-longitude grid, only those aggregate NCOMP points that contained at least 80% water clouds, based on the Enterprise Cloud Type, were included. While this limited the number of points, it did provide good comparison opportunities as the accuracy of these matches is -6.05 gm^{-2} and -9.02 gm^{-2}, respectively, while the precision is 22.09 gm^{-2} and 23.76 gm^{-2}, respectively, all meeting the F&PS requirement of 25 gm^{-2} for accuracy and 25 gm^{-2} for precision. Greenwald et al. (2007) explore the uncertainties in the AMSR-E LWP retrievals, which are fairly large, so this result is encouraging despite the somewhat large precision values.

a) Nadir-only   b) Full swath
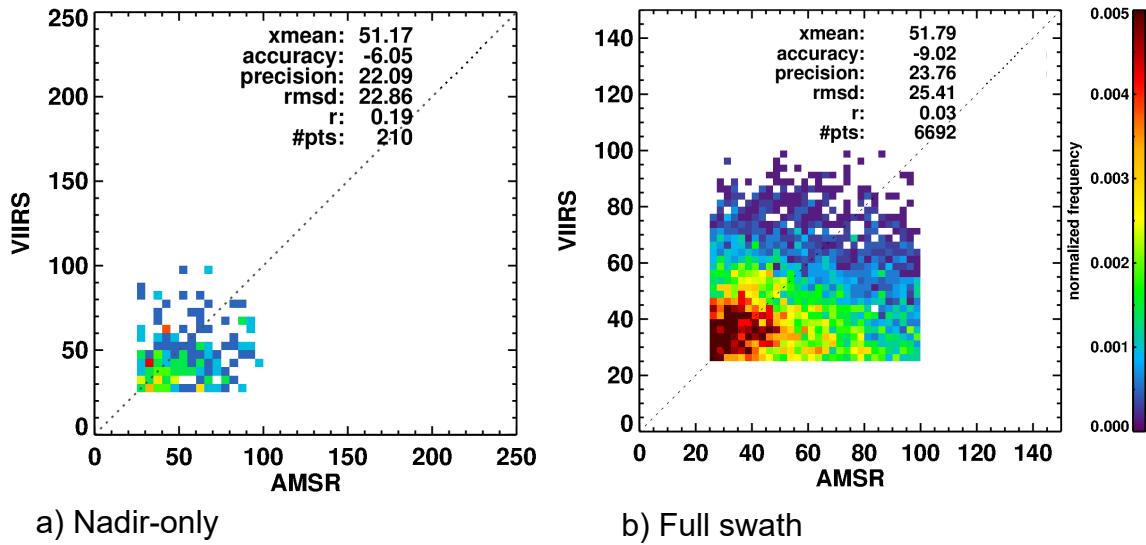
Figure 24. Retrievals of liquid water path (gm^{-2}) from matched AMSR-2 and NCOMP from a subset of SNPP VIIRS imagery during the 2.5-month validation period.

LWP and IWP from CloudSat was also compared to NCOMP during the same period. As with CloudSat CPS and COD, the RO limitations of CloudSat, as well as NCOMP's own uncertainty of 40%, are expected to limit the potential for these comparisons, yet LWP for GOES-R Cloud Type water yielded a bias of 14.0 g/m2 or 18.2% with accuracy of 24.9 g/m2 or 37.7%. While these LWP results are within the F&PS criteria, the number of samples was only 116 and perhaps fortuitous, so the AMSR-E comparisons from Fig. 24 are used in assessing NCOMP's LWP performance. As expected and as noted by Zhang and Mace (2006) who found theoretical RO IWP uncertainties of 40 to 50% , IWP comparisons with CloudSat yielded less impressive results.

The aforementioned linkage of LWP, CPS and COD indicates that those quantities proving difficult to validate, namely CPS and IWP, are expected to meet GOES-R specifications. Given that LWP is meeting F&PS criteria, despite thin water clouds often proving difficult for remote sensing techniques to quantify, we anticipate that if a sufficient source of surface data is identified, water cloud CPS and COD will compare well. Similarly, the ice cloud COD comparisons with Calipso, the gold standard sensor

for thin ice clouds, are meeting specifications, so we anticipate that ice cloud CPS, hence IWP will also meet specifications.

Bolstering our validation is also possible by running the JPSS algorithms on MODIS or GOES data, thereby greatly increasing the availability of surface sites that have MWR and MWR-radar combinations from which COD, CPS, LWP and IWP can be derived. Once those capabilities are available, these additional validations will be conducted.

6   ASSUMPTIONS AND LIMITATIONS

The following sections describe the current limitations and assumptions in the current version of the NCOMP.

6.1   Performance

The following assumptions have been made in developing and estimating the performance of the NCOMP. The following list contains the current assumptions and proposed mitigation strategies.

1. NWP data of comparable or superior quality to the current 6 hourly GFS forecasts are available. (Use longer range GFS forecasts or switch to another NWP source – ECMWF).

2. RTM calculations are available for each pixel. (Use reduced vertical or spatial resolution in driving the RTM).

3. All of the ancillary data is available at the pixel level. (Use larger scale ancillary date sets).

4. The 3.9µm, 11µm and 12µm channels are available.

6.2   Assumed Sensor Performance

We assume the sensor will meet its current specifications. However, the NCOMP will be dependent on the following instrumental characteristics.

1. Unknown spectral shifts in some channels will cause biases in the clear-sky RTM calculations and in the accuracy of the emittance parameterizations, which may impact the performance of the NCOMP.

2. Errors in navigation from image to image will affect the accuracy of clear sky temperatures that are used in the retrieval scheme.

As discussed earlier, calibration differences will be closely monitored.

6.3 Pre-Planned Product Improvements

The NCOMP development is tied to the development of other Enterprise algorithms. At this point, it is therefore difficult to predict what the future modifications will be. However, the following list contains our current best guess of the future NCOMP modifications.

6.3.1 Addition of Other Wavelengths

It is surmised that use of the 8.5- and 13.3-µm channels can provide additional information that can be exploited to improve the NCOMP retrievals (e.g., Takano et al., 1992; Strabala et al., 1994). Currently at NASA Langley, modifications to the SIST using the 8.5- and 13.3-µm channels are being studied, although usage of other channels cannot be ruled out. Results of those analyses using ABI, VIIRS and MODIS data will determine whether or not the NCOMP will be modified. Use of additional wavelengths may allow NCOMP to determine optical depths for optically thicker clouds and may reduce inaccuracies in optical depth and particle size, hence LWP and IWP.

6.3.2 Multi-layer Clouds

The NCOMP's performance in situations with multi-layer clouds will be explored. If it is possible to include recent innovations in detecting multiple cloud layers (Chang et al., 2009) and the properties of the respective layers, then those techniques will be streamlined and adapted for NCOMP usage.

6.3.3 Parameterization Updates

The emittance parameterizations will be updated using the NPP VIIRS filter functions rather than GOES filter functions. Additionally, the usage of new ice crystal models that include rough crystals will be explored. Both of these should result in improved cloud optical depths and particle sizes. To maintain consistency with the daytime retrievals, a completely new set of models will also be developed that uses the official Cloud AWG ice crystal model set for VIIRS and ABI retrievals. They will be thoroughly tested and validated as well as produced in-house by NASA Langley.

7 REFERENCES

Baum, B.A., P. F. Soulen, K. I. Strabala, M. D. King, S. A. Ackerman, and W. P. Menzel, Remote sensing of cloud properties using MODIS Airborne Simulator imagery during SUCCESS, 2000. II. Cloud thermodynamic phase. *J. Geophys.Res.,* **105**, 11,781-11,792.

Chang, F.-L., P. Minnis, B. Lin, M. Khaiyer, R. Palikonda, and D. Spangenberg, 2009: A modified method for inferring cloud top height using GOES-12 imager 10.7- and 13.3-μm data. Submitted to *J. Geophys. Res.*

Chiriaco, M., H. Chepfer, P. Minnis, M. Haeffelin, S. Platnick, D. Baumgardner, P. Dubuisson, M. McGill, V. Noel, J. Pelon, D. Spangenberg, S. Sun-Mack, and G. Wind, 2007: Comparison of CALIPSO-like, LaRC, and MODIS retrievals of ice cloud properties over SIRTA in France and Florida during CRYSTAL-FACE. *J. Appl. Meteorol. Climatol*., **46**, 242-272.

Chiriaco, M., H. Chepfer, V. Noel, A. Delaval, M. Haeffelin, P. Dubuisson, and P. Yang. 2004. Coupling infrared radiometer and lidar observations for retrieving semi-transparent cirrus cloud particle size. *Mon. Wea. Rev.*, **132**, 1684-1700.

Dong, X., and G. G. Mace, 2003: Profiles of low-level stratus cloud microphysics deduced from ground-based measurements. *J. Atmos. Oceanic Tech.*, **20**, 42-53.

Downing, H. D. and D. Williams, 1975: Optical constants of water in the infrared. *J. Geophys. Res*., **80**, 1656-1661.

Greenwald, T. J., T. S. L'Ecuyer, and S. A. Christopher, 2007: Evaluating specific error characteristics of microwave-derived liquid water cloud products. *Geophys. Res. Lett.*, 34, L22807, doi:10.1029/2007GL031180.

Hansen, M., R. DeFries, J.R.G. Townshend, and R. Sohlberg, 1998: UMD Global Land Cover Classification, 1 Kilometer, 1.0, Department of Geography, University of Maryland, College Park, Maryland, 1981-1994.

Illingworth, A. J., and Co-authors, 2007: CLOUDNET, continuous evaluation of cloud profiles in seven operational models using ground-based observations. *Bull. Amer. Meteorol. Soc.*, **88**, 883-898.

Katagiri, S. and T. Nakajima, 2004: Characteristics of cirrus clouds as retrieved from AVHRR. *J. Meteorol. Soc. Japan*, **82**, 81-89.

Lin, X., and J. A. Coakley, 1993: Retrieval of properties for semitransparent clouds from multispectral infrared imagery data. *J. Geophys. Res*., **98**, 18,501-18,514.

Liu, C.-L., and A. J. Illingworth, 2000: Toward more accurate retrievals of ice water content from radar measurements of clouds. *J. Appl. Meteorol.*, **39**, 1130-1146.

Mace, G. G., Y. Zhang, S. Platnick, M. D. King, P. Minnis, and P. Yang, 2005: Evaluation of cirrus cloud properties from MODIS radiances using cloud properties derived from ground-based data collected at the ARM SGP site. *J. Appl. Meteorol.*, **44**, 221-240.

Minnis, P., L. Nguyen, W. L. Smith, Jr., R. Palikonda, D. R. Doelling, J. K. Ayers, Q. Z. Trepte, and F.-L., Chang, 2006: MSG SEVIRI applications for weather and climate: Cloud properties and calibrations. *Proc. 3rd MSG RAO Workshop*, (ES SP-619) Helsinki, Finland, June 15, 25-30.

Minnis, P., D. P. Garber, D. F. Young, R. F. Arduini, and Y. Takano, 1998: Parameterization of reflectance and effective emittance for satellite remote sensing of cloud properties. *J. Atmos. Sci.*, **55**, 3313-3339.

Minnis, P., D. P. Kratz, J. A., Jr. Coakley, M. D. King, D. Garber, P. Heck, S. Mayor, D. F. Young, and R. Arduini: Cloud Optical Property Retrieval (Subsystem 4.3). "Clouds and the Earth's Radiant Energy System (CERES) Algorithm Theoretical Basis Document, Volume III: Cloud Analyses and Radiance Inversions (Subsystem 4)", NASA RP 1376 Vol. 3, edited by CERES Science Team, December, 1995, pp. 135-176.

Minnis, P., K. N. Liou, and Y. Takano, 1993: Inference of cirrus cloud properties using satellite-observed visible and infrared radiances. Part I: Parameterization of radiance fields. *J. Atmos. Sci.*, **50**, 1279-1304.

Minnis, P., and Co-authors, 2009: CERES Edition-2 cloud property retrievals using TRMM VIRS and Terra and Aqua MODIS data – Part I. *IEEE Trans. Geosci. Remote Sens.*, **49**, 4374-4400.

Minnis, P., and P. W. Heck, 2010: Nighttime Cloud Optical Depth, Cloud Particle Size, Cloud Ice Water Path, andn Cloud Liquid Water Path. *Algorithm Theoretical Basis Document*, NOAA NESDIS STAR. **50**.

Seemann, S.W., E. E. Borbas, R. O. Knuteson, G. R. Stephenson, and H.-L. Huang, 2007: Development of a global infrared land surface emissivity database for application to clear sky sounding retrievals from multi-spectral satellite radiance measurements. *J. Appl. Meteorol. Climatol.*, **47**, 108–123

Smith, W. L., P. Minnis, H. Finney, R. Palikonda, and M. M. Khaiyer, 2008: An evaluation of operational GOES-derived single-layer cloud top heights with ARSCL over the ARM Southern Great Plains site. *Geophys. Res. Lett.*, **35**, L13820, doi:10.1029/2008GL034275.

Strabala, K. I., S. A. Ackerman, and W. P. Menzel, 1994: Cloud properties inferred from 8–12-μm data. *J. Appl. Meteor.,* **33,** 212–229.

Takano, Y., Liou, K. N. and P. Minnis, 1992: The effects of small ice crystals on cirrus infrared properties. *J. Atmos. Sci.*, **49**, 1487-1493.

Takano, Y. and K. N. Liou, 1989: Radiative transfer in cirrus clouds I. Single scattering and optical properties of oriented hexagonal ice crystals. *J. Atmos. Sci.*, **46**, 3-20.

Turner, D. D. and R. E. Holz, 2005: Retrieving cloud fraction in the field-of-view of a high-spectral-resolution infrared radiometer. *Geosci. Remote Sens. Lett.*, **3**, 287-291.

Warren, S. G., 1984: Optical constants of ice from the ultraviolet to the microwave. *Appl. Opt*., **23**, 1206-1224.

Zhang, Y. and G. Mace, 2006: Retrieval of cirrus microphysical properties with a suite of algorithms for airborne and spaceborne lidar, radar, and radiometer data. *J. Appl. Meteor. Clim.*, **45**, 1665-1689.

Appendix 1: Lagrangian N-Points Interpolation Scheme

A1.1 INTERPOLATION OF EMISSIVITY ON NATURAL LOG COD

An interpolation scheme for obtaining a cloud emissivity between COD nodes that uses a Lagrangian N-Points Interpolation technique is detailed below. This scheme is used when an emissivity has already been calculated for each of the 8 COD nodes and a candidate COD has been calculated and input. Note that the interpolation is done in natural log of COD.

Given (1) Num_COD_Bins, the number of COD bins in the emissivity models, (2) Emiss (Num_COD_bins), the cloud emissivity for each COD bin, and (3), COD, the candidate cloud optical depth, this logic computes Emiss_Cloud, the cloud emissivity at the input optical depth.

Important internal quantities:
   Ki, which is the starting bin to use in the interpolation
   Kf, which is the ending bin to use in the interpolation
   Log_COD_Nodes(Num_COD_Bins) – these values are preset to the
        natural log of each COD bin
   Weights(Num_COD_Bins) – these are the computed weights for each COD bin
      that are used in computing Emiss_Cloud.

If the candidate COD is greater than 0.0, then attempt the interpolation. If the candidate COD is less than or equal to 0.0, then return a value of 0.0 for the emissivity.

First convert the input COD to natural log using

   Log_COD = natural log (COD).

If Log_COD is less than or equal to the smallest of the Log_COD_Nodes, then use the emissivity from the smallest COD bin with the contribution from cloud opacity included, i.e.,

   Emiss_Cloud = 4.0 * COD * Emiss (1).

Note that when referring to COD bins in this section, it refers to the COD bins of the Log_COD_Nodes array.

If Log_COD is greater than or equal to the largest of the COD bins, then use the emissivity from the largest COD bin, i.e.,

Emiss_Cloud = Emiss (Num_COD_Bins)

Otherwise, find the nodes for interpolation between COD bins using Lagrangian N-Point Interpolation scheme. First, determine the indices that will bracket the interpolation using the logic in Appendix 1.2.

Assuming that the minimum and maximum nodes of the interpolation, Ki and Kf, respectively, have been determined, then first verify that Ki and Kf are not equal, which would indicate no interpolation is necessary, hence Emiss_Cloud would be assigned the value of Emiss_Cloud(Ki).

If Ki and Kf are not equal, then the interpolation will use all bins between COD bins Ki and Kf, inclusive. First, compute

Delta = Abs((Emiss(Kf) - Emiss(Ki)) / (Emiss(Kf) + Emiss(Ki)))

If Delta is greater than 0.005, then check the value of Ki. If Ki is the first bin, then set Kf so that the first 4 COD bins are used, i.e., Ki = 1 and Kf = 4. Additionally, if Delta is greater than 0.005, Ki is not equal to 1, and Kf is the equal to the number of COD bins, then set Ki so that the last 4 bins are used, i.e., Ki = 5. On the other hand, if Delta is greater than 0.005, Ki is not equal to 1, and Kf is not the equal to the number of COD bins, then expand Ki and Kf so that an extra bin is used on each side, i.e., Ki = Ki - 1 and Kf = Kf + 1.

Now that Ki and Kf are set, it is necessary to use the logic of Appendix 1.3 to obtain the weights for each COD bin used in the interpolation. After these weights are obtained, the desired cloud emissivity at the input COD can be calculated by summing the product of each emissivity associated with COD bins Ki to Kf with its corresponding weight.

A1.2 OBTAINING NODES FOR THE N-POINTS INTERPOLATION

In order to obtain the nodes for the Lagrange N-points interpolation between COD bins, the following binary search logic is used. For a strictly monotonic vector, X, of length Num_X and a desired independent value, Xo, for which interpolation indices are desired, the indices, Ki and Kf, the minimum and maximum indices, respectively, are determined.

First, the quantity ((Xo - X(1)) * (Xo – X(Num_X)) determines whether or not the binary search is to be done. If that quantity is greater than 0.0 the search is not conducted.

If the search is not conducted and both the difference between the values of X at the largest and smallest nodes is less than 0.0, and the difference between the value of X at the first node and Xo is less than or equal to 0.0, then the quantity L is set to 1. Similarly, if the search is not conducted and both the difference between the values of X at the

largest and smallest nodes is greater than or equal to 0.0, and the difference between the value of X at the first node and Xo is greater than or equal to 0.0, then the quantity L is set to 1. If neither of those conditions is met when the search is not being conducted, then L is set to Num_X.

Ki is then set to L – 1. If Ki is less than 1, then it is reset to 1. Kf is set to Ki + 1, but if that value of Kf is greater than Num_X, then Ki is reset to Num_X – 1 and Kf is reset to Ki + 1 and those values are used as the nodes in Appendix 1.1.

If, however, the binary search method is used to find the value of L, the following branched if logic is used to find L with the sensitivity to the magnitude of the interpolated data, Epsilon, set to 1.E-6.

```
        Mk = 0
        I = 1
        L = Num_X
        M = Num_X
        IF (Xo - X(1)) 1,2,3
1       CONTINUE
        K = -1
        GOTO 4
2       CONTINUE
        Mk = 1

        Exit Search

3       CONTINUE
        ! start with K = 1
        K = 1

4       CONTINUE

        D = Xo - X(M)
        IF (K < 0) D = -D
        IF (Abs(D) < Epsilon) GOTO 6
        IF (D) 5,6,7
5       CONTINUE
        L = M
        GOTO 8
        ! if here then Mk = M
6       CONTINUE
        Mk = M

        Exit Search
```

```
7    CONTINUE
     I = M
8    CONTINUE
     M = (I + L) / 2
     IF (M /= I) GOTO 4
```

If M is indeed equal to I, at this point, just as above, Ki is then set to L − 1. If Ki is less than 1, then it is reset to 1. Kf is set to Ki + 1, but if that value of Kf is greater than Num_X, then Ki is reset to Num_X − 1 and Kf is reset to Ki + 1 and those values are used as the nodes in Appendix 1.1.

If at anytime in the search Mk has been assigned a value, then the search is exited and Ki and Kf are both set to Mk. Those values of Ki and Kf are used as the nodes in Appendix 1.1. This condition can occur in two places, both indicated by "Exit Search" in the pseudo code above.

A1.3 OBTAINING WEIGHTS FOR THE N-POINTS INTERPOLATION

The logic below describes the method for obtaining the weights for each COD bin involved in the Lagrangian 2-point or 4-point interpolation on a fixed interval of natural log (2.0) ranging from natural log (0.25) to natural log (32.0). Given the target value Xa, in this case natural log (COD), Ki and Kf, the starting and ending bin numbers, respectively, the weights for each COD bin are determined. The weights are computed and stored in an array of dimension 8 that corresponds to the weights to be used in the interpolation. Note that all values are not necessarily used since Ki and Kf determine how many nodes are used.

Important internal quantities:
    X – an array with values preset to the natural log of each COD bin

    D0 = 0.6931472
    Di = 1.442695
    Dj = 1.501390
    Dk = 0.5004635

If Kf is equal to Ki + 1, the 2-point interpolation is used, i.e., Weight(Ki) is set to the quantity X(Kf) – Xa multiplied by Di from above and Weight(Kf) is set to the quantity 1.0 = Weight(Ki).

Otherwise, the 4-point interpolation scheme is used, as described by the equations below

    D4 = Xa - X(Kf)
    D3 = D4 + D0

D2 = D3 + D0
D1 = D2 + D0
D12 = D1 * D2
D34 = D3 * D4

and the four weights are then computed as follows:

Weights(Ki) = -D2 * D34 * Dk
Weights(Ki+1) = D1 * D34 * Dj
Weights(Ki+2) = -D12 * D4 * Dj
Weights(Kf) = D12 * D3 * Dk

At this point, the Weights for nodes Ki through Kf have been determined, using either 2- or 4-point Lagrangian interpolation and are returned to the logic of Appendix 1.1.

A1.4 INTERPOLATION OF CLOUD TEMPERATURE ON NATURAL LOG COD

The logic described below is a variation of the interpolation technique described in Appendix 1.1. This version, like Appendix 1.1, also obtains a cloud emissivity between COD nodes using an N Points Lagrangian Interpolation technique, but this variation is used only for 3.7 μm when a candidate COD is > 4.0. This version interpolates in cloud temperature rather than emissivity, but then converts the resultant temperature to emissivity. As with the emissivity interpolations, this scheme is used when an emissivity has already been calculated for each of the 8 COD nodes and a candidate COD has been calculated and input. Note that the interpolation is still done in natural log of COD.

First, the upwelling 3.7-μm radiance from below the cloud (surface + atmosphere) and the 3.7-μm cloud radiance are computed and/or referenced if they are already available. For each of the COD nodes, a corresponding total 3.7-μm cloud radiance emitting from the top of the cloud is then computed utilizing the node cloud emissivities and the below cloud and cloud radiances. The reverse fast Planck function converts the total emitting radiance at the top of the cloud to $T_{3.7}$ for each node. These node values of $T_{3.7}$ are then used in place of cloud emissivities in the interpolation scheme, as further described below.

Note that once the interpolation is accomplished, a $T_{3.7}$ solution has been obtained for the input COD. This solution is then used to compute the equivalent between-node cloud emissivity, again using the upwelling 3.7-μm radiance from below the cloud (surface + atmosphere) and the interpolated $T_{3.7}$ solution.

Below is the interpolation scheme itself, analogous to the interpolation of emissivity on natural log of COD in Appendix 1.1.

Given (1) Temp_Clear, the upwelling 3.7-μm radiance from below the cloud (surface + atmosphere) converted to temperature, (2) Num_COD_Bins, the number of COD bins in the emittance models, (3) Temp_For_COD_Bins(num_COD_bins), the temperature at top of cloud for each COD bin, i.e., $T_{3.7}$ converted to temperature, and (4) COD, the candidate cloud optical depth, this logic computes Temp_Cloud, the cloud temperature at the input optical depth.

Important internal quantities:
   Ki, the starting bin to use in the interpolation
   Kf, the ending bin to use in the interpolation

   Arrays:
    Log_COD_Nodes(Num_COD_Bins) – these values are preset to the
     natural log of each COD bin
    Weights(Num_COD_Bins) – these are the weights for each COD bin
     that are used in computing Temp_Cloud.

If the candidate COD is greater than 0.0, then attempt the interpolation. If the candidate COD is less than or equal to 0.0, then the returned cloud temperature is set to Temp_Clear.

In order to attempt the interpolation, first convert the input COD to natural log using

   Log_COD = natural log (COD).

If Log_COD is less than or equal to the smallest of the Log_COD_Nodes, then use the top of the cloud temperature from the smallest COD bin with the contribution from the surface and cloud included, i.e.,

   Temp_Cloud = Temp_Clear + 4. * COD * (Temp_For_COD_Bins(1) – Temp_Clear)

Note that when referring to COD bins in this section, it refers to the COD bins of the Log_COD_Nodes array.

If Log_COD is greater than or equal to the largest of the COD bins, then use the cloud temperature from the largest COD bin, i.e.,

   Temp_Cloud = Temp_For_COD_Bins (Num_COD_Bins)

Otherwise, find the nodes for interpolation between COD bins using Lagrangian N-Point Interpolation scheme. First, determine the indices that will bracket the interpolation using the logic in Appendix 1.2.

Assuming that the minimum and maximum nodes of the interpolation, Ki and Kf, respectively, have thus been determined, then first verify that Ki and Kf are not equal,

which would indicate no interpolation is necessary, hence Temp_Cloud would be assigned the value of Temp_Cloud(Ki).

If Ki and Kf are not equal, then the interpolation will use all bins between COD bins Ki and Kf, inclusive. First, compute

Delta = Abs((Temp_For_COD_Bins (Kf) - Temp_For_COD_Bins (Ki)) /
       (Temp_For_COD_Bins (Kf) + Temp_For_COD_Bins(Ki)))

If Delta is greater than 0.01, then check the value of Ki. If Ki is the first bin, then set Kf so that the first 4 COD bins are used, i.e., Ki = 1 and Kf = 4. Additionally, if Delta is greater than 0.01, Ki is not equal to 1, and Kf is the equal to the number of COD bins, then set Ki so that the last 4 bins are used, i.e., Ki = 5. On the other hand, if Delta is greater than 0.01, Ki is not equal to 1, and Kf is not the equal to the number of COD bins, then expand Ki and Kf so that an extra bin is used on each side, i.e., Ki = Ki - 1 and Kf = Kf + 1.

Now that Ki and Kf are set, it is necessary to use the logic of Appendix 1.3 to obtain the weights for each COD bin used in the interpolation. After these weights are obtained, the desired cloud temperature at the input COD can be calculated by summing the product of each cloud temperature associated with COD bins Ki to Kf with its corresponding weight.

Appendix 2: Calculation of Emittance Using Parameterization Coefficients

The following describes the method of computing the emittance for a particular combination of ζ, ξ and μ in Equation (9) and includes additional information about the form of the coefficients in the input data file. The computation logic uses coefficients from fits to emittance values for three different channels (3.7 or 3.9, 10.8 and 12.0 μm) and computes an emittance array, Emissivity, corresponding to a fixed array of optical depths for clouds as a function of cloud model index, IM, cosine viewing zenith angle, CVZ, clear temperature, CLR, and cloud temperature, CLD.

As mentioned in 3.3.2, the coefficients are stored in 3 arrays, one each for VIIRS channel 3.9μm, 11μm and 12μm, which correspond to the aforementioned wavelengths. Similarly, the array names use the suffixes "_a", "_b" and "_c" in their names, also corresponding to those VIIRS channels. Each channel set contains 3840 coefficients. Q_Coef_Chn_a is the full set of coefficients for 3.9μm while the sets for channels 11μm and 12μm are Q_Coef_Chn_b and Q_Coef_Chn_c, respectively.

For the purposes of example, note that the location Q_Coef_Chn_a (2, 20, 7) refers to the 3.9μm coefficients for

COD bin (2), i.e., COD = 0.5,

coefficient bin (20)

and Model bin (7), i.e., water radius = 32 μm.

The sets of 30 coefficients are stored and read using a single array index, i.e, Ndq above, to minimize the number of array indices and to facilitate coding, The 30 elements are later mapped to the proper values of i, j, and k from Eq. 9 with values ranging from 0 to 2, 0 to 4 and 0 to 1, respectively, using a procedure described below. This remapping is a part of the coefficient ollapsing scheme, also detailed below.

Collapsing scheme and emittance calculation example for the 3.9μm:

Since ε_λ in Equation (9) is a function of ζ, ξ and μ, whenever a new value of either of those variables is encountered in the iteration process, the corresponding contribution from coefficients d_{ijk}, ζ, ξ and/or μ need to be recomputed to obtain the emittance for the eight optical depth nodes and the phase-appropriate CPS model. If, however, not all of those values of ζ, ξ and μ have changed in successive computations of emittance, then only the appropriate components of Eq. 9 need to change. For example, given that for all computations of emittance for a particular pixel have the same μ, the j components of d_{ijk} and μ are invariant, hence the contribution of μ is calculated only upon the first requirement for a cloud emittance for a particular CPS model for that pixel. When T_{cld} and/or T_{cs} change for a particular pixel and model, the appropriate portions of d_{ik} and either ζ and ξ will be recomputed, but the j components will remain the same. The 30 coefficients, d_{ijk}, and the contribution of ζ, ξ and μ for each COD and CPS model can thus be collapsed into subsets to increase efficiency whenever possible.

It is important to note that in fact, for a given VIIRS pixel not only is μ invariant, but so are the NCOMP input value T_{cld} and the value T_{cs}, which is derived from the input value T_s or the input RTM TOA radiance, hence ζ and ξ also do not change. Their collective invariance means that the scheme for computing the contribution of coefficients d_{ijk} and ζ, ξ and μ will be used only once per pixel, although it is necessary to retain the flexibility of piecemeal collapsing should future versions of NCOMP need to vary T_{cld} and/or T_{cs}.

All 3 channels use the same method for collapsing and computing the coefficients and ζ, ξ and μ, with the only exception being a small variation for the 3.7 or 3.9-μm channel, as noted below. The pseudo code that follows can be used for either one of the three channels, but the example presented is for 3.7 or 3.9 μm with the variation noted.

Given (1) Num_Mdls, the total number of models, currently 16, (2) Mdl_Num, the model number used for the calculation, currently from 1 to 16, (3) Cos_View_Zen_Ang, the cosine of the viewing zenith angle, (4) Temp_Clr, the temperature at the bottom of the cloud, including surface and atmosphere contributions, (5) Temp_Cld, the cloud

temperature, (6) Num_OD_Bins, the number of COD bins, currently eight, and (7) Q_Coef_Chn_a, the 3840 coefficients read from the input date file, this logic will compute the modeled cloud emissivity for each COD bin for the model Mdl_Num and store those emissivities in an array, Emissivity (Num_OD_Bins).

Remapping to i, j and k:

As previously mentioned, the sets of 30 emittance parameterization coefficients are stored in a single array index. These sets are remapped to appropriate values of i, j and k in Equation (9) using the scheme below, where Ni, Nj and Nk are equivalent to the maximum values of i, j and k, respectively, from Equation (9).

> Nip=Ni+1
> Nkp=Nk+1
> Njp=Nj+1
> Nds=Nip
> Ndr=Nds*Nkp
> Ndq=Ndr*Njp

These values are left as variables should the parameterization for future instruments change and because it facilitates the indexing of the collapsing scheme. Note that although Ndq is computed above, it has been assumed earlier to equal 30 for the purposes of inputting the coefficient arrays.

The real array R_Coef_Chn_a (Num_OD_Bins, Ndr, Num_Mdls) will contain collapsed versions of the input coefficient array with the contribution of cosine viewing zenith angle to d_{ijk} included. Note that Ndr is computed above.

The real array S_Coef_Chn_a (Num_OD_Bins, Nds, Num_Mdls) contains collapsed versions of the input coefficient array with the contribution of the 1.0 / Alog(Temp_Clr) terms, along with the R_Coef_Chn_a portion, to d_{ijk} included. Note that Nds is computed above.

The real array T_Coef_Chn_a (Num_OD_Bins, Num_Mdls) contains collapsed versions of the input coefficient array with the contribution of the 1.0 / Alog(Temp_Clr – Temp_Cld) terms and the S_Coef_Chn_a portion, to d_{ijk} included.

Cos_View_Zen_Ang_Old_Chn_a (Num_Mdls), Temp_Clr_Old_Chn_a (Num_Mdls) and Temp_Cld_Old_Chn_a (Num_Mdls) are arrays that store μ, Temp_Cld and Temp_Clr, respectively, from the previous invocations of this logic. Temp_Cld and Temp_Clr are T_{cld} and T_{cs} as defined below Eq. 9. They are all preset to -999.0 when a pixel is first processed by NCOMP. If either of these three has changed when a particular model is utilized, the appropriate portion of the coefficient and either Temp_Cld or Temp_Clr are recomputed. Additionally, the values of R_Coef_Chn_a, S_Coef_Chn_a and T_Coef_Chn_a are saved in memory whenever the routine is exited so that they can be

used in the determination of emissivity should their contribution to the computation not vary with subsequent invocations of the scheme:

To generate reduced arrays for channel a, i.e., VIIRS channel 3.9MM, a change in the Cos_View_Zen_Ang is first evaluated. If the input Cos_View_Zen_Ang is not the same as the Cos_View_Zen_Ang_Old_Chn_a for the same Mdl_Num, then R_Coef_Chn_a is recomputed, Cos_View_Zen_Ang_Old_Chn_a is set to Cos_View_Zen_Ang and both Temp_Clr_Old_Chn_a (Num_Mdls) and Temp_Cld_Old_Chn_a (Num_Mdls) are set to - 999.0, hence initiating their recomputation too.

For each optical depth bin OD_Idx, we calculate R_Coef_Chn_a as follows:

For each Ii from 0 to the maximum number of i in Equation (8),

    Qii = 1+Ii

    DO Kk = 0, Nk
       Qkk = Kk*Nip
       Pik0 = Qii+Qkk*Njp
       Pik1 = Pik0+Nip
       Pik2 = Pik1+Nip
       Pik3 = Pik2+Nip
       Pik4 = Pik3+Nip
       R_Coef_Chn_a (OD_Idx, Qii+Qkk, Mdl_Num) =
          Q_Coef_Chn_a(OD_Idx, Pik0, Mdl_Num) +
          Cos_View_Zen_Ang * (Q_Coef_Chn_a (OD_Idx, Pik1, Mdl_Num) +
          Cos_View_Zen_Ang * (Q_Coef_Chn_a (OD_Idx, Pik2, Mdl_Num) +
          Cos_View_Zen_Ang * (Q_Coef_Chn_a (OD_Idx, Pik3, Mdl_Num) +
          Cos_View_Zen_Ang * (Q_Coef_Chn_a (OD_Idx, Pik4, Mdl_Num)))))
   ENDDO.

If the input Cos_View_Zen_Ang is the same as the Cos_View_Zen_Ang_Old_Chn_a for the same Mdl_Num, then there is no need to recompute R_Coef_Chn_a .

Similarly, we then check for a change in Temp_Clr. If the input Temp_Clr is not the same as the Temp_Clr_Old_Chn_a for the same Mdl_Num, then S_Coef_Chn_a is recomputed, Temp_Clr_Old_Chn_a is set to Temp_Clr and Temp_Cld_Old_Chn_a(Num_Mdls) is set to -999.0, hence initiating its recomputation too.

If S_Coef_Chn_a is being recomputed, we set Ra equal to the value 1.0 / Alog(Temp_Clr) and then for each optical depth bin OD_Idx, we calculate S_Coef_Chn_a as follows:

For each Ii from 0 to the maximum number of i in Equation (8),

Qi = 1+Ii
S_Coef_Chn_a (OD_Idx, Qi, Mdl_Num) =
    R_Coef_Chn_a (OD_Idx, Qi, Mdl_Num) +
    Ra*R_Coef_Chn_a (OD_Idx, Qi + Nip, Mdl_Num)

Similarly, we then check for a change in Temp_Cld. If the input Temp_Cld is not the same as the Temp_Cld_Old_Chn_a for the same Mdl_Num, then T_Coef_Chn_a is recomputed and Temp_Cld_Old_Chn_a is set to Temp_Cld.

The following small exception that applies only to channel 3.9MM is contained in this paragraph. For only this channel, should Temp_Cld be greater than Temp_Clr, then for each optical depth bin T_Coef_Chn_a is set equal to 1.0 and the remaining computation of T_Coef_Chn_a is skipped.

Otherwise, to calculate T_Coef_Chn_a first Da is set equal to the value 1.0 / Alog(Amax1(3.0, Temp_Clr - Temp_Cld)), where Alog is natural log and Amax1 determines the maximum of the two numbers, and then for each optical depth bin OD_Idx, we calculate T_Coef_Chn_a as follows:

  T_Coef_Chn_a (OD_Idx, Mdl_Num) = S_Coef_Chn_a(OD_Idx, 1, Mdl_Num) +
    Da*(S_Coef_Chn_a (OD_Idx, 2, Mdl_Num) +
    Da*(S_Coef_Chn_a (OD_Idx, 3, Mdl_Num)))

T_coef_Chn_a now contains the cloud emissivity for each COD bin, so the Emissivity output array can be filled with the corresponding T_Coef_Chn_a values.

Appendix 3: Common Ancillary Data Sets

1. LAND_MASK_NASA_1KM

a. Data description

Description: Global 1km land/water used for MODIS collection 5
Filename: lw_geo_2001001_v03m.nc
Origin: Created by SSEC/CIMSS based on NASA MODIS collection 5
Size: 890 MB.
Static/Dynamic: Static

b. Interpolation description

The closest point is used for each satellite pixel:

1) Given ancillary grid of large size than satellite grid

2) In Latitude / Longitude space, use the ancillary data closest to the satellite pixel.

2. *NWP_GFS*

a. *Data description*

Description: NCEP GFS model data in grib format – 1 x 1 degree (360x181), 26 levels
Filename: gfs.tHHz.pgrbfhh
     Where,
     HH – Forecast time in hour: 00, 06, 12, 18
     hh – Previous hours used to make forecast: 00, 03, 06, 09
Origin: NCEP
Size: 26MB
Static/Dynamic: Dynamic

b. *Interpolation description*

There are three interpolations are installed:

NWP forecast interpolation from different forecast time:

Load two NWP grib files which are for two different forecast time and interpolate to the satellite time using linear interpolation with time difference.

Suppose:

T1, T2 are NWP forecast time, T is satellite observation time, and T1 < T < T2. Y is any NWP field. Then field Y at satellite observation time T is:

$$Y(T) = Y(T1) * W(T1) + Y(T2) * W(T2)$$

Where W is weight and

$$W(T1) = 1 – (T-T1) / (T2-T1)$$
$$W(T2) = (T-T1) / (T2-T1)$$

NWP forecast spatial interpolation from NWP forecast grid points. This interpolation generates the NWP forecast for the satellite pixel from the NWP forecast grid dataset.

The closest point is used for each satellite pixel:

1) Given NWP forecast grid of large size than satellite grid
2) In Latitude / Longitude space, use the ancillary data closest to the satellite pixel.

NWP forecast profile vertical interpolation

Interpolate NWP GFS profile from 26 pressure levels to 101 pressure levels

For vertical profile interpolation, linear interpolation with Log pressure is used:

Suppose:

y is temperature or water vapor at 26 levels, and y101 is temperature or water vapor at 101 levels. p is any pressure level between p(i) and p(i-1), with p(i-1) < p <p(i). y(i) and y(i-1) are y at pressure level p(i) and p(i-1). Then y101 at pressure p level is:

y101(p) = y(i-1) + log(p[i] / p[i-1]) * (y[i] – y[i-1]) / log (p[i] / p[i-1])

3. SFC_TYPE_AVHRR_1KM

a. *Data description*

Description: Surface type mask based on AVHRR at 1km resolution
Filename: gl-latlong-1km-landcover.nc
Origin: University of Maryland
Size: 890 MB
Static/Dynamic: Static

b. *Interpolation description*

The closest point is used for each satellite pixel:

1) Given ancillary grid of large size than satellite grid
1) In Latitude / Longitude space, use the ancillary data closest to the satellite pixel.

4. SFC_EMISS_SEEBOR

a. *Data description*

Description: Surface emissivity at 5km resolution
Filename: global_emiss_intABI_YYYYDDD.nc
       Where, YYYYDDD = year plus Julian day
Origin: UW Baseline Fit, Seeman and Borbas (2006).
Size: 693 MB x 12
Static/Dynamic: Dynamic

b. *Interpolation description*

The closest point is used for each satellite pixel:

1) Given ancillary grid of large size than satellite grid
2) In Latitude / Longitude space, use the ancillary data closest to the satellite pixel.

5. CRTM

a. Data *description*

Description: Community radiative transfer model
Filename: N/A
Origin: NOAA / NESDIS
Size: N/A
Static/Dynamic: N/A

b. Interpolation *description*

A double linear interpolation is applied in the interpolation of the transmissitance and radiance profile, as well as in the surface emissivity, from four nearest neighbor NWP grid points to the satellite observation point. There is no curvature effect. The weights of the four points are defined by the Latitude / Longitude difference between neighbor NWP grid points and the satellite observation point. The weight is defined with subroutine ValueToGrid_Coord:

NWP forecast data is in a regular grid.

 Suppose:
Latitude and Longitude of the four points are:

(Lat1, Lon1), (Lat1, Lon2), (Lat2, Lon1), (Lat2, Lon2)

Satellite observation point is:

(Lat, Lon)

Define

$aLat = (Lat – Lat1) / (Lat2 – Lat1)$

$alon = (Lon – Lon1) / (Lon2 – Lon1)$

Then the weights at four points are:

$w11 = aLat * aLon$

$w12 = aLat * (1 – aLon)$

$w21 = (1 – aLat) * aLon$

$w22 = (1-aLat) * (1 – aLon)$

Also define variable at the four points are:

$a11, a12, a21, a22$

Then the corresponding interpolated result at satellite observation point (Lat, Lon) should be:

$$a(Lat, Lon) = (a11*w11 + a12*w12 + a21*w21 + a22*w22) / u$$

Where,

$$u = w11 + w12 + w21 + w22$$

c. CRTM calling procedure in the AIT framework

The NWP GFS pressure, temperature, moisture and ozone profiles start on 101 pressure levels.

They are converted to 100 layers in subroutine Compute_Layer_Properties. The layer temperature between two levels is simply the average of the temperature on the two levels.

$layer\_temperature(i) = (level\_temperature(i) + level\_temperature(i+1))/2$

While pressure, moisture and ozone are assume to be exponential with height.

$hp = (log(p1)-log(p2))/(z1-z2)$

$p = p1* exp(z*hp)$

Where p is layer pressure, moisture or ozone. p1,p2 represent level pressure, moisture or ozone. z is the height of the layer.

CRTM needs to be initialized before calling. This is done in subroutine Initialize_OPTRAN. In this call, you tell CRTM which satellite you will run the model. The sensor name is passed through function call CRTM_Init. The sensor name is used to construct the sensor specific SpcCoeff and TauCoeff filenames containing the necessary coefficient

data, i.e. seviri_m08.SpcCoeff.bin and seviri_m08.TauCoeff.bin. The sensor names have to match the coefficient file names. You will allocate the output array, which is RTSolution, for the number of channels of the satellite and the number of profiles. You also allocate memory for the CRTM Options, Atmosphere and RTSoluiton structure. Here we allocate the second RTSolution array for the second CRTM call to calculate derivatives for SST algorithm.

Before you call CRTM forward model, load the 100-layer pressure, temperature, Moisture and ozone profiles and the 101 level pressure profile into the Atmosphere Structure. Set the units for the two absorbers (H_2O and O_3) to be MASS_MIXING_RATIO_UNITS and VOLUME_MIXING_RATIO_UNITS respectively. Set the Water_Coverage in Surface structure to be 100% in order to get surface emissivity over water. Land surface emissivity will be using SEEBOR. Also set other variables in Surface data structure, such as wind speed/direction and surface temperature. Use NWP surface temperature for land and coastline, and OISST sea surface temperature for water. Set Sensor_Zenith_Angle and Source_Zenith_Angle in Geometry structure. Call CRTM_Forward with normal NWP profiles to fill RTSolution, then call CRTM_Forward again with moisture profile multiplied by 1.05 to fill RTSolution_SST. The subroutine for this step is Call_OPTRAN.

After calling CRTM forward model, loop through each channel to calculate transmittance from each level to Top of Atmosphere (TOA). What you get from RTSolution is layer optical depth, to get transmittance
 Trans_Atm_Clr(1) = 1.0

```
 Do Level =  2 , TotalLevels
    Layer_OD = RTSolution(ChnCounter, 1)%Layer_Optical_Depth(Level
-1)
    Layer_OD = Layer_OD /
COS(CRTM%Grid%RTM(LonIndex,LatIndex) &
                %d(Virtual_ZenAngle_Index)%SatZenAng * DTOR)
   Trans_Atm_Clr(Level) = EXP(-1 * Layer_OD) &
                * Trans_Atm_Clr(Level - 1)
 ENDDO
```
DTOR is degree to radius PI/180.
Radiance and cloud profiles are calculated in Clear_Radiance_Prof
```
 SUBROUTINE Clear_Radiance_Prof(ChnIndex, TempProf, TauProf,
RadProf, &
                 CloudProf)
 B1 = Planck_Rad_Fast(ChnIndex, TempProf(1))
 RadProf(1) = 0.0_SINGLE
 CloudProf(1) = B1*TauProf(1)
```

```
 DO LevelIndex=2, NumLevels
   B2 = Planck_Rad_Fast(ChnIndex, TempProf(LevelIndex))
   dtrn = -(TauProf(LevelIndex) - TauProf(LevelIndex-1))
   RadProf(LevelIndex) = RadProf(LevelIndex-1) +
(B1+B2)/2.0_SINGLE * dtrn


   CloudProf(LevelIndex) = RadProf(LevelIndex) +
B2*TauProf(LevelIndex)
   B1 = B2
 END DO
```

Transmittance, radiance and cloud profiles are calculated for both normal CRTM structure and the 2nd CRTM structure for SST.

Call Clear_Radiance_TOA to get TOA clear-sky radiance and brightness temperature.

```
SUBROUTINE Clear_Radiance_TOA(Option, ChnIndex, RadAtm,
TauAtm, SfcTemp, &
                   SfcEmiss, RadClr, BrTemp_Clr, Rad_Down)
IF(Option == 1) THEN
  IF(PRESENT(Rad_Down))THEN
    RadClr = RadAtm + (SfcEmiss * Planck_Rad_Fast(ChnIndex,
SfcTemp) &
          + (1. - SfcEmiss) * Rad_Down) * TauAtm
  ELSE
    RadClr = RadAtm + SfcEmiss * Planck_Rad_Fast(ChnIndex,
SfcTemp) &
             * TauAtm
  ENDIF

  CALL Planck_Temp(ChnIndex, RadClr, BrTemp_Clr)

 ELSE
   RadClr = 0.0
   BrTemp_Clr = 0.0
ENDIF
```

In this subroutine, Rad_Down is optional, depending on if you want to have a reflection part from downward radiance when you calculate the clear-sky radiance. Notice that clear-sky radiance and brightness temperature on NWP grid only calculated for normal CRTM structure not the SST CRTM structure.

Also save the downward radiances from RTSolution and RTSolution_SST to CRTM_RadDown and CRTM_RadDown_SST. Save CRTM calculated surface emissivity to CRTM_SfcEmiss. The above steps are done in subroutine CRTM_OPTRAN